HIGHLY EXPLOSIVE 2010 MERAPI ERUPTION: EVIDENCE FOR SHALLOW-LEVEL CRUSTAL ASSIMILATION AND HYBRID FLUID

Anastassia Y. Borisova [1, 2*], Caroline Martel [3], Sophie Gouy[1], Indyo Pratomo [4], Sri Sumarti[5], Jean-Paul Toutain[6], Ilya N. Bindeman[7], Jean-Philippe Metaxian[8], Surono[9]

[1] *Géosciences Environnement Toulouse, Observatoire Midi-Pyrénées, Université Toulouse III/CNRS/IRD/CNES, GET UMR 5563, 14 Avenue E. Belin, 31400 Toulouse, France (anastassia.borisova@get.obs-mip.fr)*

[2] *Geological Department, Moscow State University, Vorobevu Gory, 119899, Moscow, Russia*

[3] *Université d'Orléans - CNRS/INSU ISTO, UMR 7327 Orléans, France (cmartel@cnrs-orleans.fr)*

[4] *Museum Geologi, Pusat Survei Geologi, Jln. Diponegoro No. 57, Bandung, Indonesia (indyopratomo@gmail.com)*

[5] *Volcano Investigation and Technology Development Institution, Yogyakarta, Indonesia (martisumarti@yahoo.com)*

[6] *Institut de Recherche pour Développement, IRD, Indonesia (jean-paul.toutain@ird.fr)*

[7] *Geological Sciences, University of Oregon, Eugene, Oregon, USA (bindeman@uoregon.ed)*

[8] *Institut des Sciences de la Terre – Université de Savoie (metaxian@univ-savoie.fr)*

[9] *Center of Volcanological and Geological Hazard Mitigation, Bandung, Indonesia (surono@vsi.esdm.go.id)*

* Corresponding author: *Géosciences Environnement Toulouse, Observatoire Midi-Pyrénées, 14 Avenue E. Belin, 31400 Toulouse, France* anastassia.borisova@get.obs-mip.fr; Tel: +(33)561332631; *Fax:* +(33)5 61 33 25 60

Journal of Volcanology and Geothermal Research

Special volume on the 2010 Merapi eruption

Version 1/22/2013~~1/21/2013~~

Keywords: Merapi volcano, Indonesia, subplinian eruption, ash-leachate, magmatic fluid, decarbonation, limestone assimilation mechanism, CO_2 pressure

Abstract

The processes responsible for the highly explosive events at Merapi, Central Java, Indonesia have been investigated through a petrological, mineralogical and geochemical study of the first-stage tephra and pyroclastic flows sampled in October and November 2010, and second-stage ash sampled shortly after the 5 – 6th November 2010 paroxysmal subplinian eruption. Several chemical and physical parameters suggest that the magma assimilated calc-silicate xenoliths derived from the surrounding carbonate-bearing crust (Javanese limestone). The bulk volcanic samples have highly radiogenic $^{87}Sr/^{86}Sr$ (0.70571 – 0.70598) ratios that approach the compositional field of material similar to the calc-silicate xenoliths. The 2010 plagioclase phenocrysts from the pyroclastic flow and tephra reveal anorthite cores (up to An_{94-97}) with low FeO contents (≤0.7 wt%), and ^{18}O enrichment (6.5 ‰ $\delta^{18}O$). The major and trace elements of the silicic glasses and phenocrysts (plagioclase, low-Al augite and titanomagnetite), the Sr-Nd-O isotopic compositions of the bulk samples and plagioclases erupted in 2010 can be explained by complete digestion of the 1998 calc-silicate xenoliths. The bulk assimilation proceeded through mixing between a calcic melt ("crustal assimilant", CaO up to 10.5 wt%, CaO/Al_2O_3 up to 1.2) and the deep source hydrous K-rich melt. Similarly to the 1998 and 2006 calc-silicate xenolith composition, the 2010 crustal assimilant is enriched in Mn (MnO up to 0.5 wt%), Zn, V, Sc contents. In contrast, the hydrous K-rich melt is enriched in volatiles (Cl up to 0.37 wt%, bulk H_2O+CO_2 up to 5 ± 1 wt%), Al_2O_3, TiO_2 and REE contents, consistent with their derivation from deep source. This hydrous K-rich melt may have been saturated with an aqueous fluid at about 200 MPa, a pressure consistent with the level of the crustal assimilation. The estimated in this work 15 – 40 wt% of calc-silicate material assimilated by the magma suggest liberation up to 2.1 Mt of additional CO_2 to the pre-eruptive basaltic andesite magma. Experimental leaching of the ash

samples documents the release of an aqueous fluid enriched in Cl, Na, Ca, Cd, Sb and Zn during the paroxysmal subplinian eruption. The paroxysmal eruption may have been produced by saturating the pre-eruptive basaltic andesite magma with this hybrid aqueous carbonic NaCl-HCl-rich fluid due to bulk assimilation creating high partial pressure of CO_2 at shallow crustal conditions of about 200 MPa. In contrast, mildly explosive block-and-ash flows (typical Merapi-type) may result from incomplete (selective) assimilation of the carbonate-bearing xenoliths and lower CO_2 partial pressure that may not lead to explosive degassing.

1. Introduction

Merapi volcano, Central Java, Indonesia is one of the most active volcanoes in the world and one of the most dangerous in Indonesia (3000 to 5000 fatalities since 1672; Simkin and Siebert, 2000). The recent activity of Merapi is characterized by (i) recurrent effusive growth of viscous lave domes that collapse to form concentrated pyroclastic density currents, referred to Merapi-type block-and-ash flows (*Volcanic Explosivity Index*, VEI 2, Schwarzkopf et al., 2005) and (ii) more exceptional explosive eruptions of subplinian type (VEI 3 – 4) associated with column collapse into pumice-and-ash pyroclastic flows (Voight et al., 2000). The explosive eruption of 2010 (VEI 4) and their earlier the VEI 3 – 4 events (in 1931 and 1872, and several VEI 3 eruptions between 1822 and 1872, potentially marking a change in Merapi's activity towards a more explosive behavior (cf. Gertisser and Keller, 2003a,b). This major issue must be taken into account with respect to monitoring implications, hazard analysis, and early warning protocols. Hence, a detailed study of the physical and chemical

processes leading to increased explosivity at Merapi is a prerequisite to better understand the mechanisms generating lava dome eruptions versus explosive volcanic events.

Recent investigations highlighted an important influence of subducted sedimentary material on trace element and Sr-Nd-Hf-Pb-O isotope compositions of the recent Merapi magmas (Gertisser and Keller, 2003a; Debaille et al., 2006; Handley et al., 2011), whereas detailed micro-analytical and experimental data reveal also significant effects of shallow-level assimilation with local Javanese sedimentary crust (Chadwick et al., 2007; Deegan et al., 2010; 2011; Troll et al., 2012; Troll et al., this issue). Limestone assimilation can play a key role in producing highly explosive fluid-saturated magmas (e.g., Iacono-Marziano et al., 2008; 2009; Freda et al., 2008; Mollo et al., 2010; Deegan et al., 2010; Troll et al., this issue). To investigate the impact of crustal assimilation on the magma-fluid system producing the highly explosive 2010 eruption of Merapi, we analyzed major, trace and volatile elements, as well as and Sr-Nd-Pb-O isotopes on bulk ash, tephra, pyroclastic flow products and their minerals and glasses, using state-of-the-art analytical methods. Based on the data, we propose a mechanism for crustal assimilation that preceded and triggered the 2010 Merapi paroxysmal subplinian eruption.

2. Materials and Methods

2.1. Ash, tephra and pyroclastic flow sampling

Solid tephra and blocks from pyroclastic flows (5 to 7 cm in diameter) have been sampled during the Merapi 2010 early-stage eruptions in 28/10/2010 – 02/11/2010. Ash samples have been sampled on 09/11/2010 from different geographic locations on the Merapi

slopes shortly after the paroxysmal stage of the subplinian eruption of 05-06/11/2010 (Table 1; Figure 1).

2.2. Energy dispersive spectroscopy (EDS) mapping and electron microprobe (EMP) techniques

EDS mapping and EMP analyses are performed at the GET laboratory in Toulouse (www.get.obs-mip.fr) and at ISTO (Institute des Sciences de la Terre d'Orléans) in Orléans. In Toulouse, the ash, tephra and pyroclastic samples were polished and investigated using the scanning electron microscope JEOL JSM-6360 LV with EDS coupled with the automatic analyser of particles by the program "Esprit" working in the module "Feature". The main mineral phases (low-Al augite, plagioclase and titanomagnetite) and minor mineral phases (orthopyroxene and aluminous clinopyroxene, K-feldspar, mineral SiO_2, olivine, Cl apatite) firstly identified by EDS technique in the samples have been confirmed thereafter by electron microprobe. Silicic matrix glasses were firstly analysed by electron microprobe and their contribution to the bulk samples was later re-examined among "unidentified phases" based on the EDS mapping.

Major- and minor- element compositions of glassy and microcrystalline matrix and melt inclusions as well as silicate, oxide and phosphate minerals were analysed *in situ* using a CAMECA SX-50 (GET, Toulouse), following the analytical procedures previously described in Borisova et al., (2005; 2010; 2012a,b). Major- and minor- element profiling of mineral phenocrysts was performed employing 1 to 10 micron steps between analytical spots/locations and the SAMX automation and wavelength-dispersive spectrometers. For spot analyses and mineral profiling the electron beam was set at an accelerating voltage of 15 kV

and a current of 10 – 20 nA for minerals and 10 nA for glasses with a spot diameter on the sample of 2 µm. The following synthetic or natural standards were used: albite (Na), periclase (Mg), corundum (Al), sanidine (K), wollastonite (Si, Ca), pyrophanite (Mn, Ti), hematite (Fe), chromium oxide (Cr), nickel oxide (Ni), sphalerite (Zn), graftonite (P), tugtupite (Cl) and topaz (F). The acquisition times for all analysed elements in glasses and major elements in minerals were 10 s per element on the peak and 5 s per element on the background. The analytical uncertainties and detection limits for major elements in the main minerals and glasses were similar to well-known analytical procedure using reference materials previously described in Borisova et al. (2005; 2010; 2012a). Detection limits for Cl, F, P and S in silicate glasses at these conditions were 500 ppm, 700 ppm, 300 ppm and 500 ppm, respectively. Apparent concentrations of elements (in particular, light ones) were corrected using the PAP data reduction method (Pouchou and Pichoir, 1991).

The microanalyses at the ISTO in Orléans were performed on blocks of the 2010 pyroclastic flows that have been mounted in epoxy resins and polished. The samples were first inspected using a scanning electron microscope JEOL JSM-6400. Major- element compositions of glasses (matrix and melt inclusions; Table S1 of ESM) and silicate minerals and Fe-Ti oxides were analysed by CAMECA SX-50 (ISTO-BRGM, Orléans), with the following conditions: accelerating voltage of 15 kV, a current beam of 10 nA, a counting time of 10 s on the peak and 5 s on the background. The spot size on the sample was 2 µm for the mineral phases and defocused to 8x8 µm for the glasses. The following synthetic or natural standards were used: albite (Si, Na), olivine (Mg), corundum (Al), orthoclase (K), andradite (Ca), synthetic oxide of $MnTiO_3$ (Mn, Ti) and magnetite (Fe). The analytical errors on the oxide analyses are 1 wt. % relative (%rel.) for SiO_2 and Al_2O_3, 2 %rel. for CaO, 3 %rel. for FeO, MgO, and TiO_2, and 5 %rel. for MnO, Na_2O and K_2O.

Apparent volatile contents in the glasses (summary CO_2 + H_2O) were estimated "by-difference" method using EMP data (Devine et al., 1995). The volatile content (assumed to be mainly water, see the part 4.4) is the difference to 100 wt% of the oxide EMP analyses, calibrated against hydrated standard glasses with well-known water contents (0.1, 4.4, and 6.4 wt% H_2O, determined by Karl-Fischer titration; see Scaillet et al., 1999; Borisova et al., 2005).

2.3. In situ major and trace element analyses of mineral and glasses by LA-ICP-QMS (Hobart, Australia)

Major and trace elements in the matrix glasses and minerals of ash samples were analysed using laser-ablation inductively coupled plasma mass spectrometry (LA-ICP-QMS) at Centre of Excellence in Ore Deposits (University of Tasmania in Hobart, Australia). The ash samples were analysed using a Resonetics Resolution M50 laser microprobe equipped with a Coherent 193 nm excimer laser, which is coupled to an Agilent 7500cs mass-spectrometer. Ablation was conducted in an atmosphere of pure He. Laser beam energy at the sample was set to ~ 3 J/cm^2, laser beam diameter to 44 μm, and ablation rate to 10 Hz. Helium carrier gas was mixed with Ar carrier gas outside the ablation cell. The ICP-QMS was tuned to minimize production of oxide interferences (ThO^+/Th^+ < 0.1%) and to enhance sensitivity in the middle to heavy mass range. Each analysis involved a 20 sec background acquisition (laser off), followed by 60 s of signal acquisition. The following masses have been measured: ^{7}Li, ^{11}B, ^{23}Na, ^{25}Mg, ^{27}Al, ^{29}Si, ^{39}K, ^{43}Ca, ^{45}Sc, ^{47}Ti, ^{51}V, ^{53}Cr, ^{55}Mn, ^{57}Fe, ^{59}Co, ^{60}Ni, ^{65}Cu, ^{66}Zn, ^{75}As, ^{85}Rb, ^{88}Sr, ^{89}Y, ^{90}Zr, ^{93}Nb, ^{121}Sb, ^{133}Cs, ^{137}Ba, ^{139}La, ^{140}Ce, ^{141}Pr, ^{146}Nd, ^{147}Sm, ^{153}Eu, ^{157}Gd, ^{159}Tb, ^{163}Dy, ^{165}Ho, ^{166}Er, ^{169}Tm, ^{172}Yb, ^{175}Lu, ^{178}Hf, ^{181}Ta, ^{208}Pb, ^{232}Th, ^{238}U with a dwell time of 0.015 sec on each mass. Data reduction was undertaken according to

standard methods (Longerich et al. 1996) using the "Sills" data reduction software (Guillong et al., 2008) Internal standardization was performed assuming a total sum for all major element oxides of 99 wt%. Regular precision of the major and trace element analyses by the LA ICP MS is in the limit of 5 – 10 %RSD (e.g., Guillong et al., 2008). Limits of detection are listed below: SiO_2 (0.01 wt%), TiO_2, Al_2O_3, FeO, MnO, MgO, CaO, Na_2O, K_2O (10^{-3} – 10^{-5} wt%), B (1.2 – 1.3 ppm), Li, Cr, Ni, Cu, Zn (~10^{-1} ppm), Sc, V, Co, Rb, Sr, Zr, Nb, Sb, Cs, Ba, La, Nd, Sm, Gd, Dy (~10^{-2} ppm), Y, Ce, Pr, Eu, Tb, Ho, Er, Tm, Yb, Lu, Ta, Th ,U (~10^{-3} ppm).

2.4. Volatile, major, trace element and Sr-Nd-Pb measurement in the bulk samples

The bulk volatile concentrations of CO_2 and S were measured at SARM (Service d'Analyse des Roches et des Minéraux at Centre de Recherches Pétrographiques et Géochimiques (CRPG) in Vandoeuvre lès Nancy, France) by Leco SC 144DR through heating at 1400°C with oxygen flux and detected by IR. The bulk H_2O concentrations were measured by Karl Ficher titration. The bulk major and trace elements were measured by ICP-OES (inductively coupled plasma atomic emission spectroscopy) and ICP-MS (inductively coupled plasma mass spectrometry) with method developed in SARM (Carignan et al., 2001) with ICP-OES IRIS Advantage ERS from Thermo Scientific and ICP-MS x7 of Thermo Scientific without pre-concentration of REE and U/Th.

For Sr-Nd-Pb isotope measurements, a special method (described below) developed in the SARM has been applied. Between 100 and 200 mg of very fine-grained powders (particle size <50 µm) were placed into 15 ml Savillex© beakers. A mixture of concentrated sub-boiled HNO_3 (4 ml) and ultrapure HF (1 ml) were added into the beakers. The solutions were heated at 115°C for 24 - 48 h, then evaporated, re-filled with concentrated HCl and heated for

24 h until complete digestion of the powder samples was achieved. The sample was then split into two parts and dried for further purification of the elements.

For Pb chromatographic separation from the matrix, 1 ml of HBr (0.8M) was added to the aliquots. The chromatographic micro-column was then filled with AG1X8 resin. The matrix was eluted with HBr (0.8M) and lead recovered with HCl 6M following a method similar to that of Manhès (1980). Isotopic analysis has been performed on a MC-ICP-MS (Isoprobe from Micromass) using Tl (NIST 997) to correct for the instrumental mass bias. Tl and Pb isotope values used for the NIST 981 and NIST 977 in this work were those obtained earlier by Thirlwall (2002). More analytical details on the applied method can be obtained in Cloquet et al. (2006). The average blanks were always negligible compared to the Pb mass used for the sample analyses and was on average below 300 pg for Pb.

For Sr and Nd isolation, the samples were diluted with 2 ml of HNO_3 (2M) following the analytical protocol of Pin et al. (1994). An additional stage for further isolation of Nd from Sm was applied using Ln spec resin following the same chemistry as described by Pin et al. (1997). Sr isotopes were measured with TIMS (Triton Plus from Thermo Electron) in the multicollection mode. Five Faraday cups were used in order to monitored Rb as well. Sr was loaded onto Re as filament. To correct for the instrumental mass bias, internal normalisation using $^{86}Sr/^{88}Sr$ (0.1194) ratio and exponential law were used. NBS 987 has been applied to control the method accuracy. The average blanks were always negligible compared to the Sr mass used for the sample analyses and was on average around 300 pg for Sr.

Nd isotopes were measured using MC-ICP-MS (Isoprobe from Micromass). To control the instrumental mass bias we used a constancy of the ratio $^{146}Nd/^{144}Nd$ (0.72190) (Luais et al., 1997) and exponential law. JMC Nd was applied to control the method accuracy. The average blank corresponded to about 100 pg for Nd and was always negligible compared to the Nd mass used for the sample analyses.

2.5. Oxygen isotopic measurement of the bulk ash samples and plagioclase fractions

Oxygen isotopic measurements were performed on 1-2 mg of plagioclase crystal fractions and ash powders using laser fluorination technique at the University of Oregon (Bindeman et al., 2008). The samples were heated with an infrared laser (9.6 μm, CO_2) in the presence of purified BrF_5 to release oxygen. Ash powders and plagioclases were not pretreated overnight to prevent room-temperature reaction, but were pretreated in a series of small increments to reduce the blank to ~0.3 micromol level. The generated O_2 gas was purified in a series of cryogenic traps held at liquid nitrogen temperature, and then a mercury diffusion pump was used to remove any remaining traces of BrF_5. Oxygen was converted to CO_2 gas by reacting with graphite at high *T* (1450°C), the yields were measured, and CO_2 was analyzed with the Isotope Ratio Mass Spectrometry (IRMS) in a dual inlet mode. Four to seven reference garnet ($\delta^{18}O$= 6.52‰, University of Oregon garnet from Gore Mt, NY, USA named as "UOG garnet") were analyzed together with the samples during each of seven analytical sessions. Day-to-day $\delta^{18}O$ variability of standards ranged from 0.1 to 0.3‰ lighter than their reference values and the measurements of unknowns were adjusted accordingly. The precision on standards is better than 0.1 ‰ of 1σ standard deviation.

2.6. Leaching experiment, ion chromatography and ICP-MS of the ash-leachates

Non-ground slightly wet ash samples have been frozen at -80° C for two reasons: (i) to avoid decomposition of possible biological material in the samples and (ii) to avoid complete loss of the volcanic fluid phase absorbed on the ash surface according to the ash leaching method revised by Witham et al. (2005). The following "freeze-dry" procedure was applied for 66 hours at GET laboratory. Two identical leaching experiments on every ash sample have been performed in distilled MQ water with solid to solution ratios ("SSR") from 1 / 24 to 1 /

18 for 28 hours following the recommendations of Witham et al. (2005). The ash-leachates were then centrifuged and filtered using 0.45 μm filters. Fluor, Cl, Br, SO_4, NO_3, NO_2 and PO_4 ion concentrations were measured by ion chromatography, using an ICS - 2000 Ion Chromatographic System with IonPac analytical column at GET. The analytical eluent was 30 mM KOH with the eluent source EGC-KOH II Cartridge. The analytical conditions were flow rate of 1 mL/min at 30°C, current of 100 mA and injection volume of 200 μL. The accuracy of the ion chromatographic method was controlled by the reference solution "CRM ION 915" (see Borisova et al., 2012b).

The HR-ICP-MS (high resolution inductively coupled plasma mass spectrometry) technique used was Element XR for metal concentration measurements in the ash leachates at GET laboratory. Two elements, of known concentrations (In and Re) were used as internal standards. The accuracy of the HR-ICP-MS method was controlled by numerous ICP-MS Certified Reference Materials. Typical accuracy, blanks and detection limits are similar those of obtained by Borisova et al. (2012b).

3. Results

3.1. Mineral and glass proportions

The results on phase proportions obtained by EDS mapping technique on the ash, tephra and pyroclastic flow samples are summarized in Table 2. The ash samples are quite homogeneous according to their mineral and glass proportions, showing more than 90 % (% refers to the surface percentage relative to the bulk surface of the investigated sample here and elsewhere in the text) of phenocryst fragments consisting of 55 to 60 % plagioclase (including anorthite), 3 to 5 % K-feldspar, 10 to 16 % clinopyroxene, 1 to 4 % orthopyroxene, 5 to 10 %

of titanomagnetite, and < 1 % olivine, apatite, and SiO_2 mineral phase. Heterogeneous matrix contains abundant bubbles and microphenocrysts (plagioclase, augite and titanomagnetite).

The consolidated tephra and pyroclastic flow samples show phenocryst contents between 26 and 65 % (depending on the sample zone) recalculated on a bubble-free basis and shows the following assemblage: 3 to 10 % plagioclase (including anorthite) up to 1700 µm size, up to 44 % orthopyroxene, 4 to 18 % clinopyroxene up to 1300 µm size, 2 to 27% titanomagnetite, < 1.5 % K-feldspar and apatite, and a single olivine and amphibole (in the pyroclastic flow samples).

Despite intensive searching, no Ca-rich metamorphic phases (e.g., wollastonite, diopside, grossular, etc.) that could have been provided from the calc-silicate xenoliths, as reported in the 1998 and 2006 products (Chadwick et al., 2007; Deegan et al., 2010), have been identified in the investigated 2010 samples (Table 2).

3.2. Bulk chemical composition (volatile, major and trace elements) of ashes, tephra and pyroclastic flow samples

The bulk 2010 ash sample chemistry summarized in Table 3 allows classifying them as basaltic andesite of the high-K series following the classification of Gertisser and Keller (2003b). The ash samples demonstrate major- and trace- element compositions typical for the Merapi volcanic series (Figures 2, 3).

3.3. Chemical composition (volatile, major and trace elements) of glasses and minerals

The melt and multi-phase inclusions (from 10 to 80 μm size and consisting of pure glass or multiphase assemblage of glass with minerals, Figure 4c) from the early-stage pyroclastic flows have heterogeneous compositions (62 – 71 wt% of SiO_2 refers to the major- and minor- element contents recalculated on the volatile-free basis here and elsewhere in the text) and variable Ca/Al ratios (CaO/Al_2O_3 = 0.08 – 1.2). The glassy melt inclusions range from Ca-poor (CaO/Al_2O_3 = 0.08) and "calcic" (CaO/Al_2O_3 = 1.2). The glassy melt inclusions from the late-stage ashes show variable SiO_2 contents (63 – 73 wt%), CaO/Al_2O_3 (0.07 – 0.14) and MnO/Al_2O_3 ratios (0.002 – 0.017), with the SiO_2-richest glasses ($SiO_2 \geq 70$ wt%) being depleted in Al_2O_3 (≤ 15.6 wt%) and CaO (≤ 1.2 wt%) relative to the "calcic" glasses (>5 wt% CaO, <13 wt% Al_2O_3, Tables 4 and S1 of ESM). Moreover, the variable Cl contents (0.06 – 0.37 wt%) are not correlated with P (0.06 - 0.39 wt%), indicating an insignificant influence of Cl-apatite crystallization on the volatile contents. Both Cl and K (3.1 – 6.6 wt% K_2O) demonstrate negative correlation with Ca contents and CaO/Al_2O_3 ratios (0.07 – 0.17; Figure 3). For example, high-K glass inclusions (analysis № 52: 6.6 wt%, 0.4 wt% of K_2O and Cl, respectively, Table S1) are poor in CaO (1.4 wt%) at ~68 wt% SiO_2, whereas some "calcic" glassy melt inclusions contain up to 10.5 wt% CaO and ~0.5 wt% MnO for SiO_2 contents of 62 – 67 wt% (Table 4).

The matrix glasses are characterized by variable SiO_2 composition (57 – 73 wt%), CaO/Al_2O_3 (0.06 – 0.48), MnO/Al_2O_3 (0.001 – 0.058) and K_2O/Al_2O_3 (0.11 – 0.44) ratios; and negative correlation of CaO/Al_2O_3 with K_2O/Al_2O_3 and positive correlation with MnO/Al_2O_3 (MnO up to 0.63 wt%) (Figure 3). The matrix glasses are characterized by high, but variable, contents of B (19.5 – 61 ppm), Ba (703 – 920 ppm), La (17 – 41 ppm), Rb (70 – 200 ppm), Th (9 – 17 ppm), Sc (2.5 – 15.6 ppm), Zn (50 – 170 ppm) and V (15 – 46 ppm, Figure 3)

relative to adakitic rhyolitic glasses (Borisova et al., 2006; 2008). Sr (140 – 413 ppm) contents in the 2010 Merapi matrix glasses overlap those experimentally synthetized (370 – 500 ppm, Deegan et al., 2010) during calc-silicate xenolith – magma interaction runs.

EMP profiling in plagioclase phenocrysts from the early-stage 2010 Merapi pyroclastic flow shows them to be strongly zoned, with cores up to 94 – 97 mol% anorthite (An_{94-97}) and rims of An_{45-50} (Figure 4a). The total range of plagioclase compositions in the 2010 samples overlap the compositional range reported for the previous eruptive events except for plagioclases richest in An and in FeO (Figure 4b). The plagioclase crystals in the late-stage ash samples are An_{48-54} with 0.04 – 0.06 wt% MgO, 0.4 – 0.5 wt% FeO, and are strongly enriched in Sr (~1000 ppm) similarly to those of analyzed by Chadwick et al. (2007). These plagioclase phenocrysts contain LREE with typical concentrations of La (4 – 7 ppm), Ce (6 – 10 ppm), Nd (2 – 4 ppm) and Rb (1 – 4 ppm).

The applied EDS mapping allows identifying two types of magmatic clinopyroxenes in the early-stage and late-stage samples: typical low-Al augites ($Al_2O_3 \leq 5$ wt%) and high-pressure aluminous clinopyroxenes (Al_2O_3 = 5 – 8 wt%). EMP analyses of low-Al augite crystals from the early-stage pyroclastic flow samples demonstrate oscillatory zonings. An example shows two positive peaks of Ti, Na and Al associated with negative peaks of Mn (Figure 4c), whereas *Mg*-number = Mg/(Mg+Fe) is broadly constant for the whole phenocryst. The low-Al augite fragments in the late-stage ash samples are rich in MnO (0.4 – 0.6 wt%), Al_2O_3 (2.7 – 3.4 wt%), Sc (~100 ppm), V (160 – 200 ppm), Zn (80 – 93 ppm), Co (35 – 39 ppm), and Sr (37 – 41 ppm) (Figure 3; Table S4 of ESM). The Fe-Ti oxides in the late-stage ash samples are titanomagnetites characterized by TiO_2 (12 – 13 wt%), MgO (~2 wt%), MnO (~1 wt%), V (3000 – 3300 ppm), Zn (1700 – 2500 ppm), and Sc (19 – 24 ppm) contents (Figure 3).

Minor mineral phases such as olivine, apatite, pargasitic amphibole, and SiO_2 mineral phases have been analyzed by different microprobe techniques (Table S5 of ESM). Olivines (Fo_{44-66}) have been found only in the ash samples and one crystal in the pyroclastic flow sample (Table 2). Apatites are ubiquitous and contain 53 – 54 wt% CaO, 41 – 42 wt% P_2O_5, and ~1 wt% Cl. Only one crystal of amphibole has been found in the block sample from the 2010 pyroclastic flows. The crystal does not show any reaction rim and has the chemical composition of pargasite (in wt%: 42 wt% of SiO_2, 11 wt% of Al_2O_3, 11 wt% of CaO, 13 wt% of FeO, 13 wt% of MgO, Table S5). The ash samples also contain 0.2 – 0.3% of a mineral of SiO_2 (97 – 99 wt% of SiO_2) enriched in Al_2O_3 (0.7 – 3.3 wt%), Na_2O (0.1 – 0.7 wt%) and K_2O (0.03 – 0.3 wt%).

3.4. Sr-Nd-Pb-O isotopic composition of ash, tephra and pyroclastic flow samples

The bulk ash samples have $^{87}Sr/^{86}Sr$ ratios of 0.70571 – 0.70575 and $^{143}Nd/^{144}Nd$ ratios of 0.51285 – 0.51294 that plot on the high- $^{87}Sr/^{86}Sr$ and low-$^{143}Nd/^{144}Nd$ end of the Merapi Sr-Nd isotopic field (Figure 5). The 2010 $^{87}Sr/^{86}Sr$ ratios in fact approach the Merapi calc-silicate xenolith field. Lead isotope ratios (Table 3) plot in the non-radiogenic side (low $^{206}Pb/^{204}Pb$) of the Merapi rock field.

Oxygen isotope compositions of plagioclase phenocryst fractions from the 2010 early-stage pyroclastic flow samples are identical: 6.5‰ for both M2010K and M2010GR. The $\delta^{18}O$ obtained for the 2010 Merapi plagioclases are comparably low values in the $\delta^{18}O$ compositional range known for plagioclases of the Holocene Pyroclastic Series ($\delta^{18}O$ = 6.5 – 7, Figure 5c). Moreover, the $\delta^{18}O$ obtained for the 2010 Merapi plagioclases plot within the common compositional range of $\delta^{18}O$ measured in the Merapi whole rocks (Figure 5c).

Oxygen isotopic composition of the bulk late-stage ash samples (average $\delta^{18}O$ is 6.5 ‰) is identical to the early-stage plagioclase composition.

3.5. Chemistry of ash-leachates

The ash-leachates produced by leaching experiments demonstrate constant F/Cl ratios (0.05 ± 0.01) and Ca-Na-Zn-Cd-Sb-Cl enrichment relative to fluid-immobile high-field strength element (HFSE: Zr, Nb, Th, Ti) normalized to the host ash composition (Figure 7). The complete compositions of the ash-leachates are given in Table S6 of ESM.

4. Discussion

4.1. Two time-constrained eruptive stages

Two main stages of eruptive activity can be distinguished based on the textural (Figure 1) and mineralogical characteristics (Table 2) of the time-constrained samples: that erupting as the early-stage tephra and pyroclastic flow and that erupting as the late-stage ashes. Rare crystals and their fragments of pure SiO_2 mineral phase, and olivine (Figure 1; Table S5 of ESM) are mostly identified in the late-stage ash samples, whereas single small fragment of olivine has been found in the early-stage pyroclastic flow sample (M2010GR, Table 2: 0.12% surface). The SiO_2 mineral phase (97 – 99 wt% of SiO_2) enriched in Al, Na and K could be either magmatic cristobalite crystallized from a silica-rich melt (Martel and Schmidt, 2003; Martel, 2012) or metamorphic quartz issued from calc-silicate xenoliths (Chadwick et al., 2007). Moreover, the Mn-rich olivines observed in the late-stage ash samples (Figure 1; MnO

= 1.2 to 1.8 wt%) also occur among the Merapi volcanic samples and are typical magmatic phases for the Merapi volcano (Figure 4d). Similarly, one euhedral pargasite crystal (~11 wt% Al_2O_3) found in the early-stage pyroclastic flows is a typical magmatic phase, since its composition (Table S5 of ESM) is compatible with crystallization from a basaltic andesite melt (53 wt. % SiO_2) at pressure ~200 MPa and temperature ~900°C (Martel et al., 2006).

Figures 3 and 5 demonstrate no geochemical difference (in trace element and Nd-Pb isotopic composition) between the 2010 Merapi early-stage and late-stage samples (Table 3), suggesting no principal difference in magmatic sources of the early and late stages. No disintegrated metamorphic crustal xenolith or mineral (derived from the metamorphic calc-silicate crust) has been identified in the 2010 samples. The main difference of the 2010 samples is their textural differences due to the type of the explosive eruption: the late-stage ash samples are fragmented and much more homogeneous (well-mixed fragments) compared to the early-stage pyroclastic flow samples (Figure 1).

4.2. Evidences for sedimentary crustal assimilation

Sedimentary crustal assimilation is an important magmatic process for the generation of the 1998 and 2006 Merapi lavas (e.g., Chadwick et al., 2007). In particular, calc-silicate xenoliths produced by contact metamorphism of the Javanese limestone crust were present in the Merapi 1998 and 2006 erupted products (Chadwick et al., 2007; Troll et al., 2012; Troll et al., this issue). These xenoliths have characteristic skarn-type mineralogy dominated by wollastonite and diopside; with lesser amounts of anorthite, quartz, Fe-oxides; and rare tremolite, grossular, apatite, titanite, calcite, larnite, and other calcium-silicate and calcium oxide minerals (Deegan et al., 2010; Borisova, personal communication). Interestingly, and

despite intensive EDS-mapping investigation, no calc-silicate xenoliths or typical phases they contain have been identified in the 2010 samples. Thus, we looked for evidence of possible pervasive crustal contamination in the 2010 products through EDS mapping, *in situ* micro-analyses of the minerals and glasses and mineral profiling.

The first line of evidences is demonstrated on figure 5(a) of the diagram of bulk-rock Sr isotope ratios versus SiO_2 contents in the Merapi pyroclastic flow and xenoliths. The radiogenic $^{87}Sr/^{86}Sr$ ratios in the 2010 samples are approaching those of the calc-silicate xenoliths. The extreme $^{87}Sr/^{86}Sr$ ratio in the 2010 bulk-rock Merapi pyroclastic flow sample (M2010 PF) is characterized by such radiogenic value as 0.706 which has never been observed yet in the pyroclastic flows of Merapi (Figure 5b).

The second line comes from the plagioclase analytical profiles, which are similar to those observed by Chadwick et al. (2007) and Deegan et al. (2010) in the 1998 Merapi lavas, i.e. plagioclase cores up to An_{94-97} and more sodic rims typically around An_{50} (Figure 4a). The first hypothesis that can be proposed to produce plagioclases with An contents > 88 mol % is crystallization from a mafic melt (SiO_2 < 56 wt%; Pichavant et al., 2002; Martel et al., 2006). Yet, such plagioclases would have FeO contents around 1 wt %, either crystallized in a deep magma chamber (~400 MPa and ~1000°C; Pichavant et al., 2002 or at shallower level (~200 MPa and ~900°C; Martel et al., 2006). Such a plagioclase would also have low $\delta^{18}O$ ratios. In contrast, the 2010 plagioclases have low FeO contents below 0.8 wt % (Figure 4a) and are enriched in ^{18}O (Figure 5c and discussion below). The 2010 Merapi phenocrysts (plagioclases and low-Al augites) were crystallized from silicic melts ($SiO_2 \geq 57$ wt%; Tables 4, S1), which is inconsistent with the origin from a "classical" basaltic melt. Since the 2010 highly calcic plagioclases approach the plagioclase compositional field typical for the Merapi calc-silicate xenoliths (Figure 4b), a second possible origin could be the metamorphic calc-silicate

xenoliths (Chadwick et al., 2007), but we did not find residual xenoliths in the 2010 products. Therefore, we propose that the highly calcic plagioclases crystallized from highly calcic melts firstly experimentally produced by Deegan et al. (2010) and described in this work for the 2010 Merapi samples (see Table 4). The calcic melts represent the "crustal assimilant" possibly produced by complete dissolution and digestion of crustal xenoliths of 1998-type upon xenolith – magma interaction, as experimentally demonstrated by Deegan et al. (2010). Moreover, high quantity of clinopyroxene, and anorthite (≥90 mol% An) fragments in the 2010 ash samples (~40 to 50 % surface and 26 – 28 % surface, respectively, Table 2) suggests abnormally Ca-enriched magma.

The third line of evidences for the early-stage crustal assimilation comes from the *in situ* measured compositions of the main phenocryst minerals (plagioclase, low-Al augite, titanomagnetite,) and matrix glasses. The matrix glasses are enriched in MnO (up to 0.4 wt%), Sr (up to ~380 ppm), Zn (up to ~170 ppm), V (up to ~160 ppm). The phenocrysts are characterized by enrichment in "vital elements" as Mn, Sr, Zn, V (Figure 3 and Tables S2 - S4 of ESM) which is typical signature of the 1998 calc-silicate xenoliths (Chadwick et al., 2007) and carbonate-bearing sediments (Brugger and Meisser, 2006; Kamber et al., 2007). The ash plagioclases are strongly enriched in Sr (typically at ~1000 ppm) at MgO = 0.04 – 0.06 wt% and FeO = 0.4 – 0.5 wt% at An_{48-54}, consistent with an assimilation and fractional crystallization process involving metamorphic crustal material.

Finally, the observed values of ^{18}O in the early-stage plagioclase phenocrysts and the bulk-rock ash samples ($\delta^{18}O^{Plag}$ = 6.5 ‰; $\delta^{18}O^{Ash}$ = 5.6 – 6.8 ‰) are lower than those characteristic for adakitic and related magmas for the 1991 Pinatubo eruption ($\delta^{18}O^{Ash}$ = 6.9 – 7.3 ‰, Fournelle et al., 1996), overlap those of basaltic andesites of the previous Merapi eruptions (Figure 5c) and are higher compared to typical mantle values ($\delta^{18}O^{MORB}$ =5.7 ‰).

The observed ^{18}O values in the early-stage plagioclase phenocrysts suggests that the 2010 Merapi plagioclase crystallized from a silicic melt contaminated by sedimentary crustal material. Calc-silicate xenoliths such as those present in the 1998 and 2006 erupted products may represent the main source of the crustal assimilant, since the xenoliths are characterized by high $\delta^{18}O$ ranging from 10 to 14 ‰ (Gertisser and Keller, 2003a; Troll et al., this issue). These metamorphic xenoliths are derived from local upper Javanese crustal limestone which is characterized by yet higher $\delta^{18}O$, ranging from 18.9 to 24 ‰ (Troll et al., this issue).

4.3. Mechanism of crustal assimilation

The *in situ* analyzed mineral and glass compositions constrain the mechanism of crustal assimilation by the pre-eruptive magmatic system. Firstly, figure 3 and table 4 demonstrate that the early-stage pyroclastic flow glasses and late-stage ash glasses of melt inclusions and matrix are heterogeneous in respect to CaO and Ca/Al, suggesting the existence of "calcic" melts representing a "crustal assimilant" at the 2010 pre-eruptive magma. High CaO and low Al_2O_3 contents are known signatures of the 1998 calc-silicate xenoliths (Figures 2, 3) and similar chemical signatures can be observed in "calcic" glassy melt inclusions trapped in low-Al augite ($Al_2O_3^{Aug}$ = 1.5 – 1.6 wt%; Table 4), suggesting their origin through melting or dissolution of calc-silicate xenoliths. High Ca/Al (CaO/Al_2O_3 >0.6), Mn (MnO = 0.1 – 0.35 wt%) coupled with variable Al (Al_2O_3 = 0.6 – 16 wt%) and low K (K_2O < 0.9 wt%,) in the calc-silicate xenoliths thus is responsible for the high CaO/Al_2O_3, MnO/Al_2O_3 and variable K_2O/Al_2O_3 in the 2010 quenched silicic glasses (Figure 3, Table 4). Secondly, the K_2O/Al_2O_3 ratio is either constant or is negatively correlated with CaO/Al_2O_3 in the melt inclusions and glassy matrix (Figure 3), suggesting two different sources of Ca and K in silicic melts. Indeed, high K contents are signatures of hydrous (Cl-rich) silicic melts issued

from deep magmatic source (analysis № 52, Table 4), whereas high Ca and Mn contents are signatures of crustal assimilant melts derived from calc-silicate xenoliths. Positive correlations of CaO/Al_2O_3 with MnO/Al_2O_3, in turn, in silicic glasses argue in favor of the binary mixing with the crustal assimilant enriched in Ca and Mn.

This mixing process can also be observed in zonation of low-Al augite phenocryst ($Al_2O_3^{Aug} \leq 3.3$ wt%) which is oscillatory for Al, Ti, Na and Mn (Figure 4c). Positive peaks in Al, Ti and Na are associated with negative peaks in Mn in the augite phenocryst. These zones likely reflect crystallization from a batch of ”pure” melt rich in alkalis, Al, Ti likely derived from a deep magmatic source rather than from sedimentary crust, i.e. less contaminated than the hybrid melts crystallizing most part of the augite phenocrystal. Moreover, the enrichment in Mn, Sr, Zn, V of the low-Al augites, as well as in the plagioclases, titanomagnetites (Figure 3; Tables S2 – S5 of ESM) and matrix glasses relative to adakitic rhyolitic melts (e.g., Borisova et al., 2006; 2008), suggest that these mineral phases were crystallized from the hybrid melt contaminated with material similar to the 1998 calc-silicate xenoliths.

On the basis of evidences, the overall analytical and microanalytical data support crustal assimilation process that proceeded through three major steps: (1) contact metamorphism of the Javanese limestone and formation of calc-silicate xenoliths of the 1998 type (not discussed here and broadly described by Chadwick et al. (2007) for Merapi and by Fulignati et al. (2005) for Vesuvius); (2) bulk assimilation of the calc-silicate xenoliths through the complete digestion, melting/dissolution and formation of the “calcic” melt end-member representing the “crustal assimilant”; (3) effective binary chemical and physical mixing of the silicate and calcic melts that carry both signatures (i.e., magmatic and crustal) and fractional crystallization of phenocrysts.

Because no information on kinetic parameters of the crustal assimilation is available (e.g., M_a and r in DePaolo, 1981 or α in Russell et al., 1995 for coupled assimilation - fractional crystallization), the pre-eruptive process of the 2010 Merapi magma assimilation can be described as an equation of binary mixing. We suggest the following equations:

$$C_{All}^{Hybr} = \text{Average}\ (C_{melt}^{Hybr}\ ;\ C_{cryst}^{Hybr}/D) = C_{melt}^{Init} \times (1 - f) + C_{melt}^{Ass} \times f \quad (1),$$

where f is fraction (f = 0 – 1) of "crustal assimilant" incorporated to the magma (hybrid melt + phenocrystals), C_{All}^{Hybr} is average concentration of an element in the bulk hybrid magmatic system C_{All}^{Hybr} = Average [C_{melt}^{Hybr}; C_{cryst}^{Hybr}], D is bulk partition coefficient between the crystals and hybrid melt ($D = C_{cryst}/C_{melt}$) and C_{melt}^{Init} is the elemental concentration in the initial melt before assimilation, C_{melt}^{Ass} is concentration of the element in the "crustal assimilant" melt.

$$\text{Therefore, } f = (\text{Average}\ [C_{melt}^{Hybr}; C_{cryst}^{Hybr}/D] - C_{melt}^{Init}) / (C_{melt}^{Ass} - C_{melt}^{Init}) \quad (2).$$

Assuming C_{melt}^{Hybr} = 214 ppm (average Sr contents in the 2010 Merapi matrix glasses, except for the maximal concentration) and bulk C_{cryst}^{Hybr} = 1063 ppm (average Sr contents in the 2010 Merapi plagioclases), C_{melt}^{Init}= 140 ppm (Sr content in a adakitic rhyolitic melt, Borisova et al., 2006; 2008) and C_{melt}^{Ass} = 380 ppm (maximal measured Sr content in the 2010 Merapi matrix glasses), D is 5.0 (partitioning between plagioclase An_{40-50} and silicic melt after Ren et al., 2003) and the equation (2), f is ~0.3.

Similarly, the pre-eruptive process of the 2010 Merapi magma assimilation can be constrained based on known Sr isotopic ratios in the bulk rocks and Sr concentrations in melts and crystals. For calculations, we adapted equation of binary mixing:

$$R_{melt}^{Hybr} = (f \times C_{melt}^{AssAll} \times R_{melt}^{Ass} + (1 - f) \times C_{melt}^{Init} \times R_{melt}^{Init}) / (f \times C_{melt}^{AssAll} + (1 - f) \times C_{melt}^{Init}) \quad (3),$$

where R_{melt}^{Init} is initial isotopic ratio in the melt before assimilation, R_{melt}^{Hybr} is isotopic ratio in hybrid melt, R_{melt}^{Ass} means isotopic ratio in "crustal assimilant" melt, C_{melt}^{AssAll} is average concentration of an element in the "crustal assimilant" melt and an element content consumed by hybrid crystals: C_{melt}^{AssAll} = Average [C_{melt}^{Ass} ; C_{cryst}^{Hybr}/D].

Therefore, $f = (C_{melt}^{Init} \times R_{melt}^{Init} - C_{melt}^{Init} \times R_{melt}^{Hybr}) / (C_{melt}^{AssAll} \times R_{melt}^{Hybr} - C_{melt}^{Init} \times R_{melt}^{Init} - C_{melt}^{AssAll} \times R_{melt}^{Ass} + C_{melt}^{Init} \times R_{melt}^{Init})$, (4).

Assuming R_{melt}^{Init} varies from 0.704 to 0.705 of $^{87}Sr/^{86}Sr$ (0.705 as the lowest Sr isotope ratio in the Merapi lavas: Figure 5; 0.704 as Sr isotope ratio in adakitic magma: Borisova et al., 2006 and references therein), R_{melt}^{Hybr} is from 0.705713 to 0.705978 for $^{87}Sr/^{86}Sr$ (Table 3), R_{melt}^{Ass} ranges from 0.707361 to 0.707866 (see calc-silicate xenolith composition, Chadwick et al., 2007) and C_{melt}^{AssAll} varies from 286 to 386 ppm and D is 5.0 and the equation (4), f ranges from 0.15 to 0.40. These estimations suggest that the pre-eruptive Merapi magma has assimilated from 15 to 40 wt% of carbonate-bearing crustal material.

4.4. Fluid phase composition and hybrid origin

The volatile contents in the silicic glasses together with the ash-leachate compositions give us first information on the composition of the magmatic fluids liberated during the late stage subplinian eruption. The melt inclusions analyzed in the ash samples exhibit high Cl contents up to 0.37 wt% (analysis № 52, Table S1), suggesting that the K-rich melt approached saturation in H_2O-Cl-bearing fluid or fluids (Cl = 0.6 – 0.9 wt% at saturation with aqueous Cl-rich fluid at 200 MPa in silicic melt; Carroll and Webster, 1994). The phenocryst-hosted K-rich melt inclusions from the early-stage pyroclastic flows are enriched in volatiles (H_2O+CO_2 regularly up to 5 ± 1 wt%, determined following the EMP by-difference method;

Figure 6), suggesting that the early-stage melts are close to be saturated with aqueous fluids at ~200 MPa (e.g., Burnham, 1994). In contrast, calcic assimilant melts are depleted in volatiles ($\leq$1.6 wt% of H_2O+CO_2 contents) relatively to the K-rich inclusions (Figure 6). The derivation of the crustal assimilant melts from carbonate-bearing xenoliths suggests their enrichment in CO_2 (CO_3^{2-}) rather than in H_2O (OH^-). Because no measurement of H_2O/CO_2 in the investigated melt inclusions has been performed quantitatively, we suggest that the upper limit of CO_2 content in the calcic melt inclusions is 1.6 wt% content (Figure 6). For all samples, most of the matrix glasses have H_2O+CO_2 contents $\leq$ 3.5 wt% (Figure 6, Table S1 of ESM), indicating progressive degassing during magma transport and subaerial emplacement.

The leaching experiments performed in this study on four ash samples (Table S6 of ESM) show constantly low F/Cl ratios (0.05 ± 0.01) and Na-Ca-Cl-Zn-Cd-Sb enrichment relative to fluid-immobile high field strength elements (HFSE: Zr, Nb, Th, Ti) (Figure 7), suggesting an aqueous Cl-rich fluid was liberated to the atmosphere during the subplinian eruption on 5-6th November 2010. Low F/Cl ratios (<0.2) strongly support an eruption of non-degassed magma typical for initial stage of subplinian explosive events (e.g., Borisova et al. 2012b). High concentrations of Zn, Cd and Sb in the ash leachates may be achieved through the equilibration of an aqueous NaCl-HCl-rich fluid with a hydrous melt enriched in these elements. According to what is known on Zn, Cd and Sb complexation with Cl in NaCl-HCl-rich fluids, their $K_d^{fluid/melt}$ should be significantly higher than 1 (Borisova et al., 2012 and references therein). According to the concept of the "geo-pH/Cl-meter" of Pokrovski et al. (2006; 2008), high HCl or an increased acidity into the aqueous phase results in formation of strong and volatile Sb-Cl ligands at the expense of Sb-OH complexes that are less stable under these conditions. This results in the preference of Sb for Cl in NaCl-HCl-rich fluids. Moreover, the saturation of the 2010 Merapi magma with Cl-rich fluids enriched in Ca, Zn and Cd can be partially related to the inferred crustal assimilation. Indeed, Zn and Cd are

known to be concentrated in oceanic carbonate-bearing sediments (Heinrichs et al., 1980). These data provide an evidence for hybrid nature of the NaCl-HCl-rich magmatic fluids liberated during the paroxysmal eruption.

The above constrained fraction of the carbonate-bearing crustal material assimilated by magma is a basis for the following estimations of the amount of CO_2 liberated at the pre-eruptive conditions. The following simplified chemical equation of decarbonation can be used: $CaCO_{3\ \text{calc-silicate xenolith}} = CO_2{\uparrow}_{\text{fluid}} + CaO_{\ \text{melt}}$ (5).

The estimated bulk mass of the volcanic material erupted in 2010 ranges from 6×10^{10} to 1.2×10^{11} kg (Surono et al., this volume). This mass of the volcanic material erupted in 2010 can be suggested as the bulk mass of magma existed at the pre-eruptive conditions. Therefore, the fraction (f) of the assimilated crustal material (0.15 – 0.40) estimated based on the equations (2) and (4), maximal contents of calcite in the calc-silicate xenoliths (5 to 10 wt% based on Borisova, personal communication) and chemical reaction (equation 5) gives 1.9×10^8 to 2.1×10^9 kg or 0.19 to 2.1 Mt of CO_2 which is equivalent from 0.3 to 3.5 wt% of an additional CO_2 in the magma (relative to the suggested mass 6×10^{10} to 1.2×10^{11} kg of the pre-eruptive magma). The upper estimate of CO_2 mass (2.1 Mt) is a factor of ~5 higher than the bulk mass of SO_2 (~0.44 Mt) liberated during the 2010 Merapi eruption (Surono et al., this volume). This maximal estimate of the liberated CO_2 mass is also in accordance with the bulk CO_2/SO_2 (7 – 115 in mol%, Surono et al., this volume) corresponding to CO_2/SO_2 (5 – 80 in wt%) measured in fumaroles before the 2010 explosive events. Thus, the additional CO_2 liberated upon the decarbonation at the pre-eruptive magma chamber has resulted in increase in partial pressure of CO_2 (see Appendix A for at least 1.5 – 10 MPa pressure of CO_2 liberated due to decarbonation depending on the suggested free volume) that was likely sufficient to trigger the explosive eruption in 2010.

4.5. *Hypothesis for triggering highly explosive eruptions at Merapi*

We propose that the paroxysmal eruption of 2010 may have resulted from the explosive degassing of a pre-eruptive magma saturated with hybrid aqueous fluids rich in NaCl-HCl and CO_2 (released due to decarbonation reaction). Such a state and maturation of the fluid phase were probably acquired because the 2010 magma completely digested an involved carbonate-bearing crust during bulk assimilation (terminology of Russell et al., 1995). In contrast, the products erupted in 1998 and 2006 contain abundant metamorphic crustal xenoliths, suggesting incomplete assimilation (selective assimilation, terminology of Russell et al., 1995) of the carbonate-bearing crust and thus lower partial pressure of CO_2 not producing the necessary conditions of fluid saturation for explosive degassing.

In a more general perspective, we propose that the bifurcation between the classical mildly explosive eruptions at Merapi (i.e. block-and-ash flows of Merapi-type) and the paroxysmal events of subplinian type may result from the efficiency of the carbonate assimilation process by Merapi magma, with incomplete (selective) assimilation leading to less explosive events and complete (bulk) assimilation triggering highly explosive eruptions. Compared to selective assimilation, bulk assimilation is the exception rather than norm (Russell et al., 1995). Such factors as kinetics of the magma – calc-silicate xenolith reaction, duration of the pre-eruptive period, volume of pre-eruptive magma and its physico-chemical properties and a contribution of basaltic end-member may potentially explain the reason of the complete (bulk) assimilation and highly explosive events.

5. Concluding remarks on the 2010 Merapi eruption

1) Although calc-silicate metamorphic minerals or xenoliths have not been observed in the 2010 eruption products, a number of geochemical signatures underline efficient crustal assimilation process. There are: (i) the highest $^{87}Sr/^{86}Sr$ ratios among the known Merapi pyroclastic rocks, (ii) high-calcic cores of plagioclase phenocrysts up to An_{94-97} with low FeO contents of 0.4 – 0.7 wt% and strong Sr enrichment up to ~1000 ppm at An_{48-54}, (iii) enrichment in ^{18}O ($\delta^{18}O$ around 6.5‰) of the bulk plagioclase phenocrysts, (iv) enrichment in Mn, Sr, Zn, V of the phenocrysts (plagioclases, low-Al augites, titanomagnetites), and (v) enrichment in Ca, Mn, Sr, Zn, V, Sc of silicic glasses in amounts comparable to the bulk 1998 calc-silicate xenoliths.

2) We propose a process of crustal assimilation through three major steps: (1) contact metamorphism of Javanese limestone and formation of the 1998 and 2006 calc-silicate xenoliths (not investigated in this work); (2) bulk assimilation through complete melting/dissolution of the calc-silicate xenoliths and production of calcic melts representing the 2010 crustal assimilant; (3) effective chemical and physical binary mixing between hydrous K-Cl-rich silicic melts issued from a deep magmatic source and the 2010 crustal assimilant melts derived from the carbonated xenoliths, and fractional crystallization of phenocrysts at pre-eruptive pressures about 200 MPa.

3) The magmatic fluid is Cl-Ca-Na-Zn-Cd-Sb-rich at the stage of the paroxysmal subplinian eruption. The saturation of the 2010 basaltic andesite magma with aqueous carbonic fluids is due to both high concentrations of NaCl and HCl in the aqueous fluid and likely CO_2 enrichment due to decarbonation of the crustal material. Such an enriched state of the magmatic fluid in CO_2 ($\geq$1.5 MPa additional pressure in the magma chamber) may be reached by complete (bulk) assimilation of the surrounding

carbonate-bearing crustal material that triggers this highly explosive event, (i.e. the paroxysmal subplinian eruption on 5-6th November 2010), whereas the classical mildly explosive eruptions at Merapi (i.e. in 1998 and 2006) may have resulted from incomplete (selective) assimilation and immature saturation state of the fluid phase.

Acknowledgements

Authors thank V. Troll, J. Webster, an anonymous reviewer for numerous suggestions improving the article and editors J.W. Neuberg and Ph. Jousset for the editorial handling. C.M. greatly thanks Ida Di Carlo for help with the SEM and EMP analyses. J.K. Russell and B.R. Edwards are thanked by A.Y.B. for fruitful discussion on the kinetics of crustal assimilation. M. Guillong and L. Danyshevsky are thanked by A.Y.B., for performing LA-ICP-MS analyses at Tasmania University (Hobart, Australia). F. Candaudap, J-F Mena and S. Mounic are thanked by A.Y.B. for performing HR-ICP-MS analyses, for the preparation of polished sections and for performing ion chromatographic methods, respectively. This work was supported by OMP (VELI, CNAP, 2011-2012) for A.Y.B. A.Y.B. is also partially supported by RFBR (number 10-05-00254).

Appendix A. Calculations of additional pressure of CO_2 liberated due to decarbonation of crustal xenoliths

To calculate pressure of the additional CO_2 liberated during decarbonation reaction, we applied the ideal gas equation: $P = R \times (n \times T / V)$ (A.1),

where P is pressure, V is free volume, R is gas constant (Boltzmann's constant), n is moles, T is temperature (K). Applying the following parameters to the equation A.1: free volume (V) equals to the suggested magma chamber volume from 0.03 to 0.06 km^3 (Surono et al., this volume, equal to $3 \times 10^{13} - 6 \times 10^{13}$ cm^3), n from 4.3×10^9 to 4.8×10^{10} moles (corresponding to the calculated mass of CO_2 1.9×10^8 to 2.1×10^9 kg = 1.9×10^{11} to 2.1×10^{12}g divided by molar mass of CO_2 = 44.01 g mol^{-1}); R = 8.314 cm^3 MPa $K^{-1}mol^{-1}$, temperature T = 1000 – 1200 °C = 1273.16 – 1473.16 K (obtained at 200 MPa according to Wells, 1977), pressure P varies from 1.5 to 10 MPa. These estimates are, however, minimal, because they depend strongly from the assumed free volume (V) in the equation (A.1).

References:

Berthommier P.C. (1990). Etude volcanologique du Merapi (Centre-Java). Téphrostratigraphie et chronologie – produits éruptifs. Thèse de Doctorat de l'Université Blaise Pascal, Clermond-Ferrand II, U.F.R. de recherche Scientifique et Technique France pp 216.

Bindeman I.N., Gurenko A., Sigmarsson O., M. Chaussidon (2008). Oxygen isotope heterogeneity and disequilibria of olivine crystals in large volume Holocene basalts from Iceland: Evidence for magmatic digestion and erosion of Pleistocene hyaloclastites Geochimica et Cosmochimica Acta 72, 4397–4420.

Borisova A.Y., Pichavant M., Beny J.-M., Rouer O., Pronost J. (2005). Constraints on degassing of dacite magma and regime of the June 15, 1991, climactic eruption of Mount Pinatubo (Philippines): New data on melt and crystal inclusions in quartz. Journal of Volcanology and Geothermal Research 145/1-2, 35-67.

Borisova AY., Pichavant M, Polvé M, Wiedenbeck M, Freydier R, Candaudap F (2006) Chemistry of silicic melts of the Mount Pinatubo, Philippines: Implications for ore-forming potential of adakitic magmatism. Geochimica et Cosmochimica Acta 70: 3702-3716.

Borisova A.Y., Freydier R., Polvé M., Salvi S., Candaudap F., Aigouy T. (2008). In situ multi-elemental analysis of the Mount Pinatubo quartz-hosted melt inclusions by NIR femtosecond laser ablation - inductively coupled plasma - mass spectrometry. Geostandards and Geoanalytical Research, 32, 209-229.

Borisova A.Y., Pokrovski G.S., Pichavant M., Freydier R., Candaudap F. (2010) Arsenic enrichment in hydrous peraluminous melts: insights from LA-ICPMS and in situ X-ray Absorption Spectroscopy. American Mineralogist, 95, 1095-1104.

Borisova A.Y., Martel C., Pratomo I., Toutain J-P., Sumarti S., Surono. (2011). "MERAPIDATA": New Petrologic and Geochemical Database of the Merapi Volcano, Central Java, Indonesia. AGU Fall Meeting. V21E-2536.

Borisova A.Y., Thomas R., Salvi S., Candaudap F., Lanzanova A., Chmeleff J. (2012a) Tin and associated metal and metalloid geochemistry by femtosecond LA-ICP-QMS microanalysis of pegmatite-leucogranite melt and fluid inclusions: new evidence for melt-melt-fluid immiscibility. Mineralogical Magazine 76, 91-113.

Borisova, A.Y., Toutain, J-P, Stefansson, A., Gouy, S., De Parseval, Ph., (2012b). Processes controlling the 2010 Eyfjallajökull explosive eruption. Journal of Geophysical Research 117, B05202, 18 pp.

Brugger J., Meisser N. (2006). Manganese-rich assemblages in the Barrhorn Unit, Turtmanntal, Central Alps, Switzerland. The Canadian Mineralogist 44, 229 – 248.

Burnham C.W. (1994). Development of the Burnham model for prediction of H_2O solubility in magmas. In: Volatiles in Magmas. Reviews in Mineralogy. (eds. M.R. Carroll and J.R. Holloway), Mineralogical Society of America. V.30, pp. 123-129.

Carignan J., Hild P., Mevelle G., Morel J., Yeghicheyan D. (2001). Routine analyses of trace elements in geological samples using flow injection and low pressure on-line liquid chromatography coupled to ICP-MS: A study of geochemical reference materials BR, DR-N, UB-N, AN-G and GH. Journal of Geostandards and Geoanalysis 25, 187-198.

Camus G., Gourgaud A., Mossand-Berthommier P.-C., Vincent P.-M. Merapi (Central Java, Indonesia): an outline of the structural and magmatological evolution, with a special emphasis to the major pyroclastic events. Journal of Volcanology and Geothermal Research, 100, 139-163.

Carroll M.R., Webster J.D. (1994). Solubilities of sulfur, noble gases, nitrogen, chlorine, and fluorine in magmas; In: Volatile in Magmas eds. Carroll M.R., Holloway J.R., Reviews in Mineralogy 30, 231-271.

Chadwick J.P., Troll V.R., Ginibre C., Morgan D., Gertisser R., Waight T.E., Davidson J.P. (2007). Carbonate assimilation at Merapi volcano, Java, Indonesia: Insights from crystal isotope stratigraphy. Journal of Petrology 48, 1793-1812.

Cloquet C., Carignan J., Libourel G. (2006). Atmospheric pollutant dispersion around an urban area using trace metal concentrations and Pb isootopic compositions in epiphytic lichens. Atmospheric Environment 40, 574-587.

Debaille V., Doucelance R., Weis D., Schiano P. (2006). Multi-stage mixing in subduction zones: Application to Merapi volcano (Java island, Sunda arc). Geochimica et Cosmochimica Acta, 70, 723-741.

Deegan F.M., Troll V.R., Freda C., Misiti V., Chadwick J.P., McLeod C.L., Davidson J.P. (2010). Magma-carbonate interaction processes and associated CO_2 release at Merapi volcano, Indonesia: Insights from experimental petrology. Journal of Petrology 51, 1027-1051.

Deegan F.M., Jolis E.M., Troll V.R., Freda C., Whitehouse M.J. (2011). Boron isotope systematics during crustal carbonate degassing. AGU Fall Meeting.

Devine J.D., Gardner J.E., Brack H.P., Layne G.D., Rutherford M.J., (1995). Comparison of microanalytical methods for estimating H_2O contents of silicic volcanic glasses. Am. Mineralogist. 80, 319-328.

Fournelle J., Carmody R., Daag A.S. (1996). Anhydrite-Bearing Pumices from the June 15, 1991, Eruption of Mount Pinatubo: Geochemistry, Mineralogy, and Petrology. In:

Newhall ChG, Punongbayan RS (eds) Fire and Mud. Eruptions and Lahars of Mt. Pinatubo, Philippines. University of Washington Press, Seattle, pp. 845-863.

Freda C., Gaeta M., Misiti V., Mollo S., Dolfi D., Scarlato P. (2008). Magma-carbonate interaction: An experimental study on ultrapotassic rocks from Alban Hills (Central Italy). Lithos 101, 397- 415.

Fulignati P., Panichi C., Sbrana A., Caliro S., Gioncada A., Del Moro A. (2005). Skarn formation at the walls of the 79 AD magma chamber of Vesuvius (Italy): Mineralogical and isotopic constraints. Neues Jahrbuch für Mineralogie 181/1.

Gertisser R., (2001). Gunung Merapi (Java, Indonisien): Eruptiongeschichte und magmatische evolution eines Hochrisiko-Vulkans. Dissertation zur Erlangung des Doktorgrades der Geowissenschaftlichen Fakultat der Albert-Ludwigs-Universitat Freiburg i Br. (CD ROM Version 12/2001). pp 1000.

Gertisser R., Keller J. (2003a). Trace element and Sr, Nd, Pb, O isotope variations in medium-K and high-K volcanic rocks from Merapi volcano, Central Java, Indonesia: Evidence for the involvement of subducted sediments in Sunda Arc magma genesis. Journal of Petrology 44, 457-489.

Gertisser R., Keller J. (2003b). Temporal variations in magma composition at Merapi volcano (Central Java, Indonesia): Magmatic cycles during the past 2000 years of explosive activity. Journal of Volcanology and Geothermal Research 123, 1-23.

Guillong M., Meier D.L., Allan M.M., Heinrich C.A., Yardley B.W.D. (2008). Sills: A MATLAB-based program for the reduction of laser ablation ICP-MS data of homogeneous materials and inclusions. Mineralogical Association of Canada Short Course 40, Vancouver, B.C., p. 328–333.

Hanley H.K., Turner S., Macpherson C.G., Gertisser R., Davidson J.P. (2011). Hf-Nd isotope and trace element constraints on subduction inputs at island arcs: Limitations of Hf anomalies as sediment input indicators. Earth and Planetary Science Letters 304, 212-223.

Heinrichs H., Schulz-Dobrick B., Wedepohl K.H. (1980). Terrestrial geochemistry of Cd, Bi, Tl, Pb, Zn and Rb. Geochimica et Cosmochimica Acta 44, 1519-1533.

Iacono-Marziano G., Gaillard F., Pichavant M. (2008). Limestone assimilation by basaltic magmas: an experimental re-assessment and application to Italian volcanoes. Contributions to Mineralogy and Petrology 155, 719-738.

Iacono-Marziano G., Gaillard F., Scaillet B., Pichavant M., Chiodini G. (2009). Role of non-mantle CO_2 in the dynamics of volcano degassing: The Mount Vesuvius example. Geology 37, 319-322.

Kamber B.S., Webb G.E. (2007). Transition metal abundancies in microbial carbonate: a pilot study based on in situ LA-ICP-MS analysis. Geobiology 5, 375 – 389.

Longerich H.P., Jackson S.E. and Günther D. (1996) Laser Ablation Inductively Coupled Plasma Mass Spectrometric Transient Signal Data Acquisition and Analyte Concentration Calculation. Journal of Analytical Atomic Spectrometry, vol. 11, 899-904.

Luais B., Telouk Ph., Albarède F. (1997). Precise and accurate neodymium isotopic measurements by plasma-source mass spectrometry. Geochimica et Cosmochimica Acta 61, 4847-4854.

Manhes G., Allegre C.J., Dupré B., Hamelin B. (1980). Lead isotope study of basic-ultrabasic layered complexes – speculations about the age of the Earth and primitive mantle characteristics. Earth and Planetary Science Letters, 47, 370-382.

Martel C. (2012) Eruption dynamics inferred from microlite crystallization experiments: Application to Plinian and dome-forming eruptions of Mt. Pelée (Martinique, Lesser Antilles). Journal of Petrology 53, 699 - 725.

Martel C., Radadi Ali A., Poussineau S., Gourgaud A., and Pichavant M. (2006) Basalt-inherited microlites in silicic magmas: evidence from Mt. Pelée (Martinique, F.W.I.). Geology 34, 905-908.

Martel C. and Schmidt B.C. (2003) Decompression experiments as an insight into ascent rates of silicic magmas. Contribution to Mineralogy and Petrology 144, 397-415.

Mollo S., Gaeta M., Freda C., DiRocco T., Misiti V., Scarlato P. (2010). Carbonate assimilation in magmas: A reappraisal based on experimental petrology. Lithos 114, 503-514.

Pichavant M., Martel C., Bourdier J.-L., and Scaillet B. (2002) Physical conditions, structure, and dynamics of a zoned magma chamber: Mount Pelée (Martinique, Lesser Antilles Arc). Journal of Geophysical Research 107, N°B5, 10.1029.

Pin C., Briot D., Bassin C., Poitrasson F. (1994). Concominant separation of strontium and samarium-neodymium for isotopic analysis in silicate samples, based on specific extraction chromatography. Analytica Chimica Acta 298, 209-217.

Pin C., Francisco J., Zalduegui S. (1997). Sequential separation of light rare-earth elements, thorium and uranium by miniature extraction chromatography: Application to isotopic analyses of silicate rocks. Analytica Chimica Acta 339, 79-89.

Pouchou J.L., Pichoir F., (1991). Quantitative analysis of homogeneous or stratified microvolumes applying the model "PAP", Electron Probe Quantitation, Eds. Heinrich and Newbury, Plenum Press N.Y., 31-75.

Pokrovski, G.S., Borisova, A.Y., Roux, J., Hazemann, J-L., Petdang, A., Tella, M. and Testemale, D. (2006) Antimony speciation in saline hydrothermal fluids: A combined X-ray absorption fine structure spectroscopy and solubility study. Geochimica et Cosmochimica Acta, 70, 4196-4214.

Pokrovski, G.S., Roux, J., Hazemann, J-L., Borisova, A.Y., Gonchar, A.A. and Lemeshko, M.P. (2008) In situ X-ray absorption spectroscopy measurement of vapor-brine fractionation of antimony at hydrothermal conditions. "Applications of synchrotron and neutron radiation in mineralogy" Special issue of Mineralogical Magazine, 72(2), 667-681.

Ren M.H., Parker D.F., White J.C. (2003). Partitioning of Sr, Ba, Rb, Y, and LREE between plagioclase and peraluminous silicic magma. American Mineralogist 88, 1091-1103.

Russell J.K., Edwards B.R., Shyder L.D. (1995). Volatile production possibilities during magmatic assimilation: heat and mass-balance constraints. In: Thompson J.F. Magmas, fluids and ore deposits. Mineralogical Association of Canada short Course Series 23, 1 – 24.

Scaillet B. and Evans B.W. (1999) The 15 June 1991 eruption of Mount Pinatubo. I. Phase equilibria and pre-erution P-T-f_{O2}-f_{H2O} conditions of the dacite magma. Journal of Petrology 40, 381-411.

Scwarzkopf L.M., Schmincke H.U., Troll V.R. (2001). Pseudotachylite on imparct marks of block surfaces in block-and-ash flows at Merapi volcano, central Java, Indonesia. Internal Journal of Earth Scinces (Geol. Rundsch.), 90, 769-775.

Scwarzkopf L.M., Schmincke H.U., Cronin S.J. (2005). A conceptual model for block-and-ash flow basal avalanche transport and deposition, based on deposit architecture of 1998 and 1994 Merapi flow. Journal of Volcanology and Geothermal Research 139, 117 – 134.

Simkin T and Siebert L. (2000) Earth's volcanoes and eruptions: an overview. In: Sigurdsson H. (ed) Encyclopedia of volcanoes, San Diego: Academic Press, p. 249-261.

Surono, Jousset P., Pallister J., Boichu M., Buongiorno M.F., Budisantoso A., Costa F., Andreastuti S., Prata F., Schneider D., Clarisse L., Humaida H., Sumarti S., Bingnami C., Griswold J., Carn S., Oppenheimer C., Lavigne F. (2012). The 2010 explosive eruption of Java's Merapi volcano – a "100-year" event. Journal of Volcanology and Geothermal Research, this issue.

Thirlwall M.F. (2002). Multicollector ICP-MS analysis of Pb isotopes using a ^{207}Pb-^{204}Pb double spike demonstrates up to 400ppm/amu systematic errors in Tl-normalization. Chemical Geology 184, 255-279.

Troll, V.R., Deegan, F.M., Jolis, E.M., Harris, C., Chadwick, J.P., Gertisser, R., Schwarzkopf, L., Borisova, A.Y., and Bindeman, I.N. (2012) Magmatic differentiation processes and their impact on eruptive behaviour at Merapi volcano: evidence from recent inclusion petrology. Journal of Volcanology and Geothermal Research, this issue.

Troll V.R., Hilton D.R., Jolis E.M., Chadwick J.P., Blythe L.S., Deegan F.M., Schwarzkopf L.M., Zimmer M. (2012). Crustal CO_2 liberation during the 2006 eruption and earthquake events at Merapi volcano, Indonesia. Geophysical Research Letters 39, L11302.

Voight B., Young K.D., Hidayat D., Subandrio, Purbawinata M.A., Ratdomopurbo A., Suharna, Panut, Sayudi D.S., LaHusen R., Marso J., Murray T.L., Dejean M., Iguchi

M., and Ishihara K. (2000) Deformation and seismic precursors to dome-collapse and fountain-collapse nuées ardentes at Merapi volcano, Java, Indonesia, 1994-1998. J. Volcanol. Geotherm. Res. 2000, 261-287.

Wells P.R.A. (1977). Pyroxene thermometry in simple and complex systems. *Contributions to Mineralogy and Petrology* **62**, 129-139.

Witham C.S., Oppenheimer C., Horwell C.J. (2005). Volcanic ash-leachates: a review and recommendations for sampling methods. Journal of Volcanology and Geothermal Research 141, 299 - 326.

FIGURE CAPTIONS

Figure 1 Photographs and photomicrographs (1) and (1a) represents an example of the 2010 Merapi ash (M2010-1) sampled. (1b) – polished ash sample M2010-1 with olivine inclusion marked in red color and investigated by EDS mapping technique; (2) - M2010-GR sample investigated by EDS mapping technique; (3a) and (3b) - M2010K pyroclastic flow sample investigated by EDS mapping technique in two zones (T1 and T2, see Table 2); (4) and (4a) - M 2010 PF sample investigated by EDS technique. The sample numbers are according to the sample numeration given in Table 1. The data obtained with the EDS mapping "Feature" are summarized in Table 2. Different colors in (2 – 4a) mark different types of phases (minerals and glasses) distinguished based on different intensity of grey tone on the back-scattered electron (BSE) images and analyzed thereafter by EDS technique. (1b). Red color on (4) marks all phases (mineral and glass) analyzed in this zone.

Figure 2. Plots showing the major- and minor- element composition of the Merapi 2010 volcanic samples compared to all available data on the Merapi volcanic rocks and calc-silicate xenoliths. The chemical data used here are obtained from MERAPIDATA (Borisova et al., 2011) which summarize the published and unpublished data of Berthommier (1990), Gertisser and Keller (2003a,b), Debaille et al. (2006), Camus et al., (2006) for the previous Merapi volcanic products; and Chadwick et al. (2007) for the 1998 Merapi calc-silicate xenoliths. The chemical data on the 2010 Merapi are given in Table 3.

Figure 3. Log-log plots of the major (wt%) and trace element contents (ppm) versus CaO/Al_2O_3 ratio in the 2010 glass inclusions, matrix glasses and phenocrysts compared to the 2010 Merapi bulk volcanic rocks and the 1998 crustal xenoliths. The chemical data on the Merapi volcanic products were obtained from database of MERAPIDATA, (Borisova et al., 2011). The database summarizes the published and unpublished data of Berthommier (1990), Gertisser and Keller (2003a,b), Debaille et al. (2006), and Camus et al. (2006) for the Merapi volcanic products; and Chadwick et al. (2007) for the 1998 Merapi calc-silicate xenoliths. The chemical data on the 2010 Merapi are given in Tables 3 and 4 and in Table S1 of ESM.

Figure 4 (a). BSE image of a plagioclase phenocryst from pyroclastic flow (M 2010 PF) and its chemical profiling for An (mol%) and FeO (wt%) from A to B points demonstrating extremely calcic core (An_{94}). The high-An core is chemical signature of assimilation of sedimentary crustal material (see text). Symmetric chemical zonation in An is spectacular. FeO contents demonstrate oscillatory zonation.

Figure 4(b). FeO (wt%) versus An (mol%) contents in the Merapi 2010 plagioclase phenocryst compared to those of typical magmatic plagioclases and calcic plagioclases from the calc-silicate xenoliths. The plagioclase composition for the Merapi volcanic products were obtained from database of MERAPIDATA (Borisova et al., 2011). The database summarizes the published and unpublished data on plagioclases of Berthommier (1990), Camus et al., (2006) for the previous Merapi volcanic products; and Chadwick et al. (2007) for the 1998 Merapi calc-silicate xenoliths. The chemical data on the 2010 Merapi plagioclases are given in Table S2 of ESM.

Figure 4 (c). BSE image of low-Al augite phenocryst from pyroclastic flow (M 2010 PF) and its chemical profiling from A to B points demonstrating oscillatory zonation in Mg index = $Mg/(Mg+Fe^{2+})$, trace TiO_2, Al_2O_3, Na_2O and MnO (wt%) contents. The Al-, Ti- and Na-enriched and Mn-depleted zones are marked. The Al- Ti- and Na-enriched zones indicate crystallization from trachyte melts enriched in alkalis and Al. Numerous inclusions in this crystal have been excluded from the phenocryst zonation. "MI" indicates the melt and multi-phase inclusions (from 10 to 80 μm size) consisting of pure glass or an assemblage of glass with minerals (plagioclase, titanomagnetite and apatite). The chemical data on the 2010 Merapi pyroxenes are given in Table S4 of ESM.

Figure 4(d). MnO (wt%) versus Fo contents (mol%) in the Merapi 2010 olivines compared to those of the typical Merapi olivines. The olivine composition for the Merapi volcanic products were obtained from database of MERAPIDATA (Borisova et al., 2011). The database summarizes the published and unpublished data on olivines of Berthommier (1990), Camus et al., (2006) for the previous Merapi volcanic products. The olivine data on the 2010 Merapi products are given in Table S5 of ESM.

Figure 5. Plots of the $^{87}Sr/^{86}Sr$ versus (a) SiO_2 in the Merapi bulk rocks; (b) versus $^{143}Nd/^{144}Nd$; (c) $\delta^{18}O$ in plagioclases and bulk rocks versus SiO_2 wt% contents in the host Merapi rocks. The 2010 Merapi products are characterized by highest $^{87}Sr/^{86}Sr$ ratios approaching those of the calc-silicate xenoliths. The isotopic data used here are obtained from MERAPIDATA (Borisova et al., 2011) which summarize the published isotopic data of Gertisser and Keller (2003a), Debaille et al. (2006) for the previous Merapi volcanic products; and Chadwick et al. (2007) for the 1998 Merapi calc-silicate xenoliths. The isotopic data on the 2010 Merapi are summarized in Table 3.

Figure 6. Plots of the (a) Cl contents (wt%) and (b) apparent H_2O+CO_2 contents (wt%) versus CaO/Al_2O_3 in glasses of melt inclusions (open circles) and glassy matrix (closed circles). Apparent H_2O+CO_2 contents in glasses are calculated by-difference method. The melt representing crustal assimilant is characterized by the highest Ca/Al (up to 1.2 of CaO/Al_2O_3), low summed H_2O+CO_2 and low Cl contents. Volatile-richest K-rich melts are characterized by low Ca/Al.

Figure 7. Diagram demonstrating the ash leachate composition normalized to the bulk ash composition for analyzed elements. Positive peaks for Zn, Cu, Cd, Sb and Cl relative fluid-immobile high-field strength elements (HFSE: Zr, Nd, Th, Ti) reflect the main elemental constituents of magmatic fluid enriched in NaCl-HCl and liberated during the paroxysmal subplinian eruption in 2010. Chemical data are given in Tables 3 and S6 of ESM.

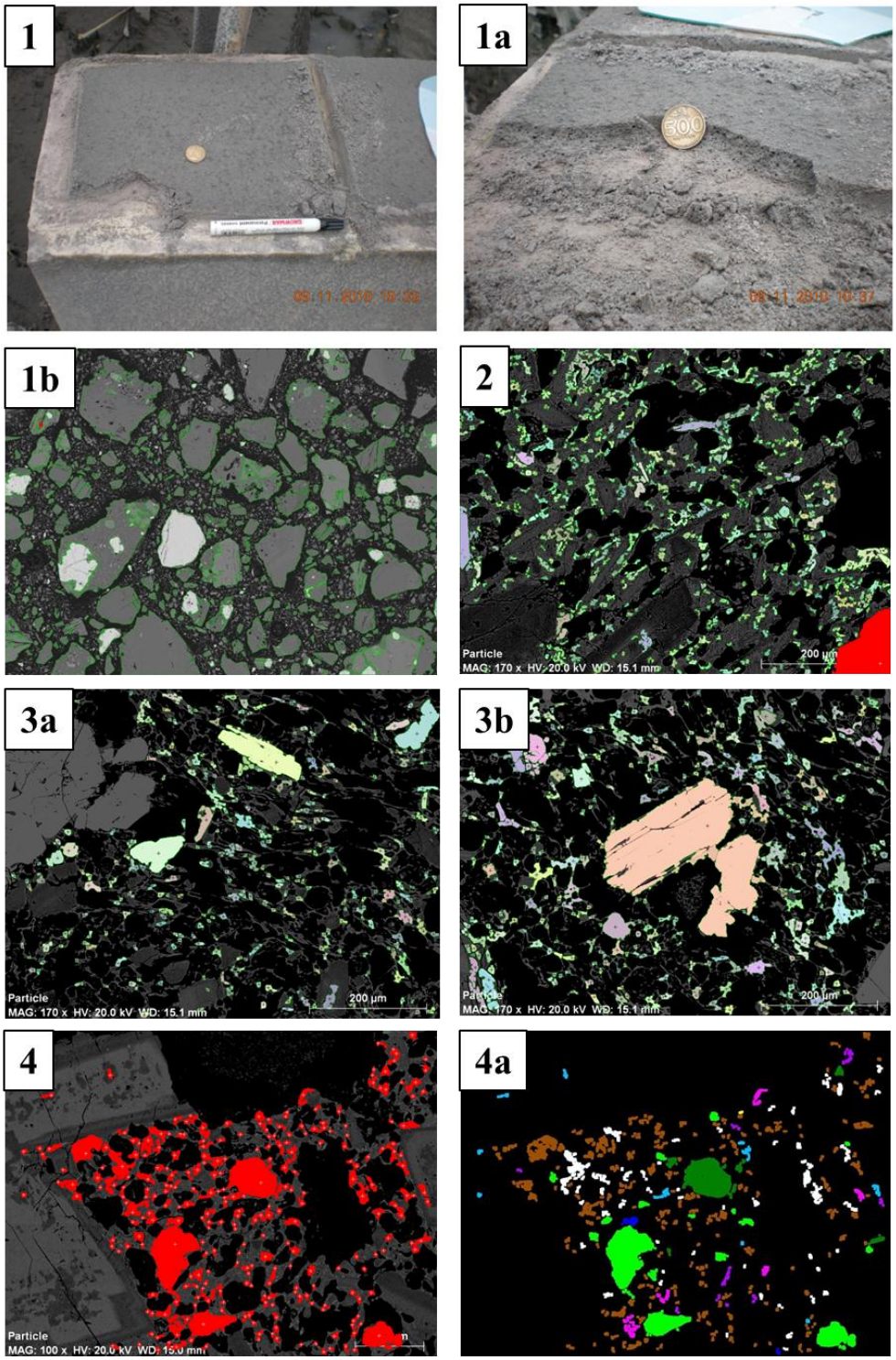

Figure 1 (1) and (1a) represents an example of the 2010 Merapi ash (M2010-1) sampling. (1b) – polished ash sample M2010-1 with olivine inclusion marked in red investigated by EDS mapping technique; (2) - M2010-GR sample investigated by EDS mapping technique; (3a) and (3b) - M2010K pyroclastic flow sample investigated by EDS mapping technique in two zones (T1 and T2, see Table 2); (4) and (4a) - M 2010 PF sample investigated by EDS technique. The sample numbers are according to the sample numeration given in Table 1. The data obtained with the EDS mapping "Feature" are summarized in Table 2.

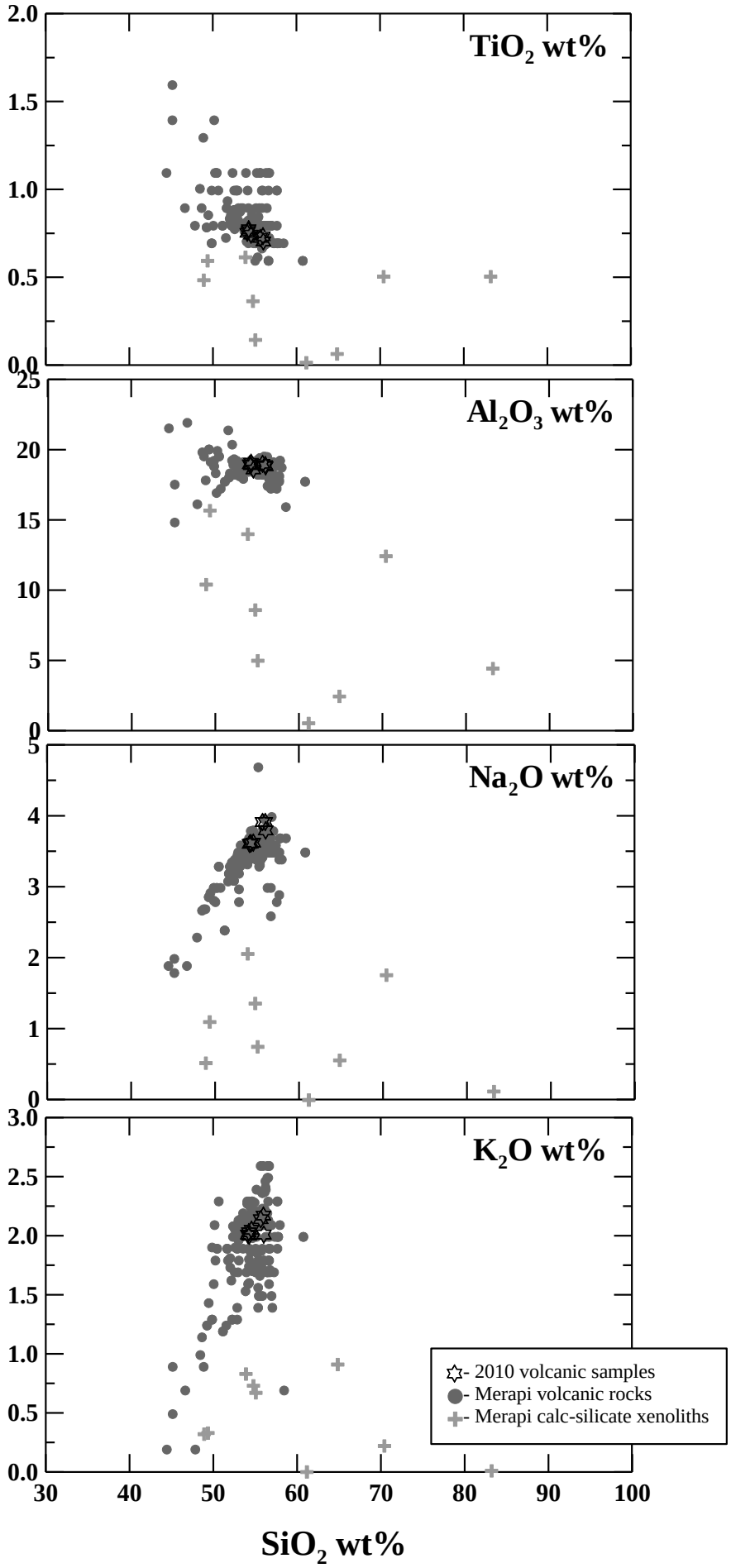
TiO2 wt%
Al2O3 wt%
Na2O wt%
K2O wt%
SiO2 wt%
- 2010 volcanic samples
- Merapi volcanic rocks
- Merapi calc-silicate xenoliths

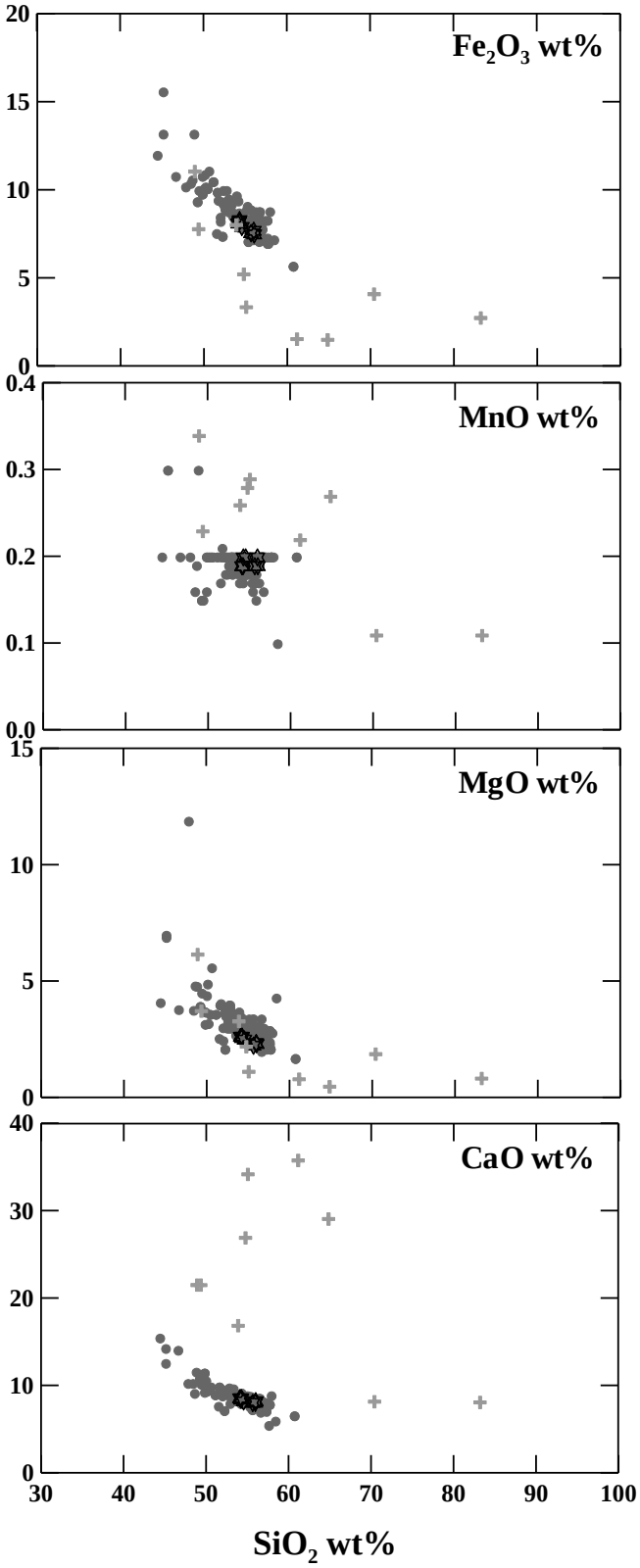

Figure 2. The major and minor element composition of the Merapi 2010 volcanic samples compared to all available data on the Merapi volcanic rocks and calc-silicate xenoliths. The chemical data used here are obtained from MERAPIDATA (Borisova et al., 2011) which summarize the published and unpublished data of Berthommier (1990), Gertisser and Keller (2003a,b), Debaille et al. (2006), Camus et al., (2006) for the previous Merapi volcanic products; and Chadwick et al. (2007) for the 1998 Merapi calc-silicate xenoliths. The chemical data on the 2010 Merapi are given in Table 3.

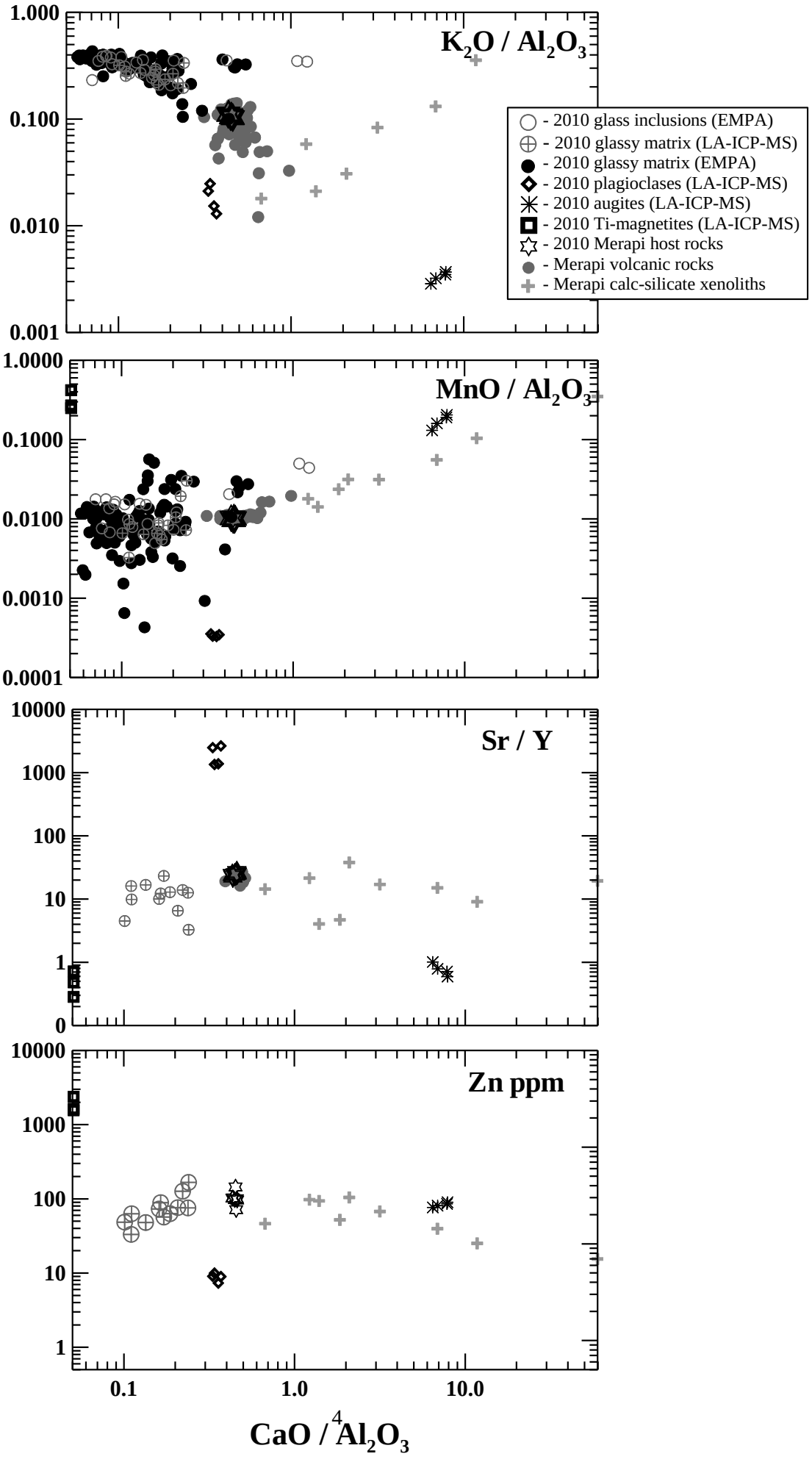
K2O / Al2O3
MnO / Al2O3
Sr / Y
Zn ppm
CaO / Al2O3
- 2010 glass inclusions (EMPA)
- 2010 glassy matrix (LA-ICP-MS)
- 2010 glassy matrix (EMPA)
- 2010 plagioclases (LA-ICP-MS)
- 2010 augites (LA-ICP-MS)
- 2010 Ti-magnetites (LA-ICP-MS)
- 2010 Merapi host rocks
- Merapi volcanic rocks
- Merapi calc-silicate xenoliths

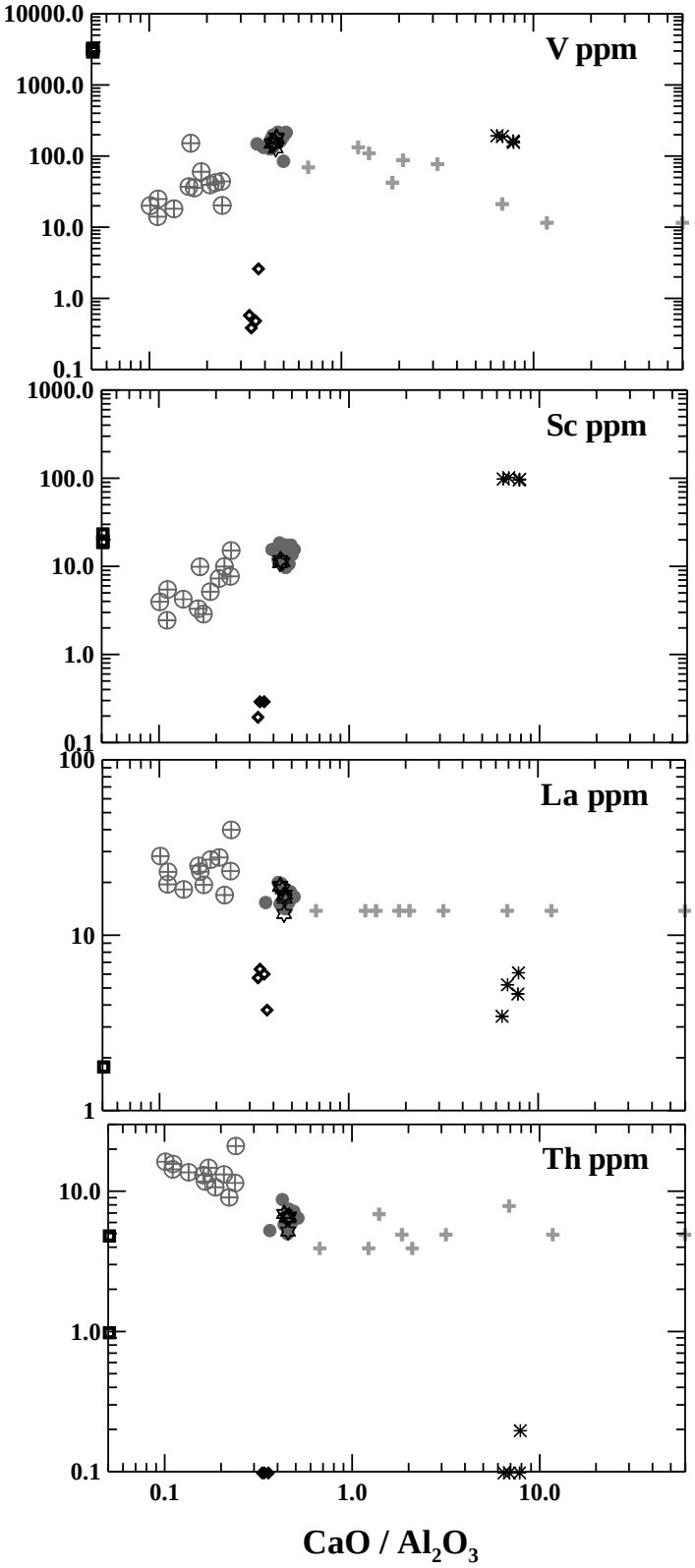

Figure 3. The major (wt%) and trace element contents (ppm) versus CaO/Al_2O_3 ratio in the 2010 glass inclusions, matrix glasses and phenocrysts compared to the 2010 Merapi bulk volcanic rocks and the 1998 crustal xenoliths. The chemical data on the Merapi were obtained from database of MERAPIDATA, (Borisova et al., 2011). The database summarizes the published and unpublished data of Berthommier (1990), Gertisser and Keller (2003a,b), Debaille et al. (2006), Camus et al., (2006) for the Merapi volcanic products; and Chadwick et al. (2007) for the 1998 Merapi calc-silicate xenoliths. The chemical data on the 2010 Merapi are given in Tables 3 and 4 and in Table S1 of ESM.

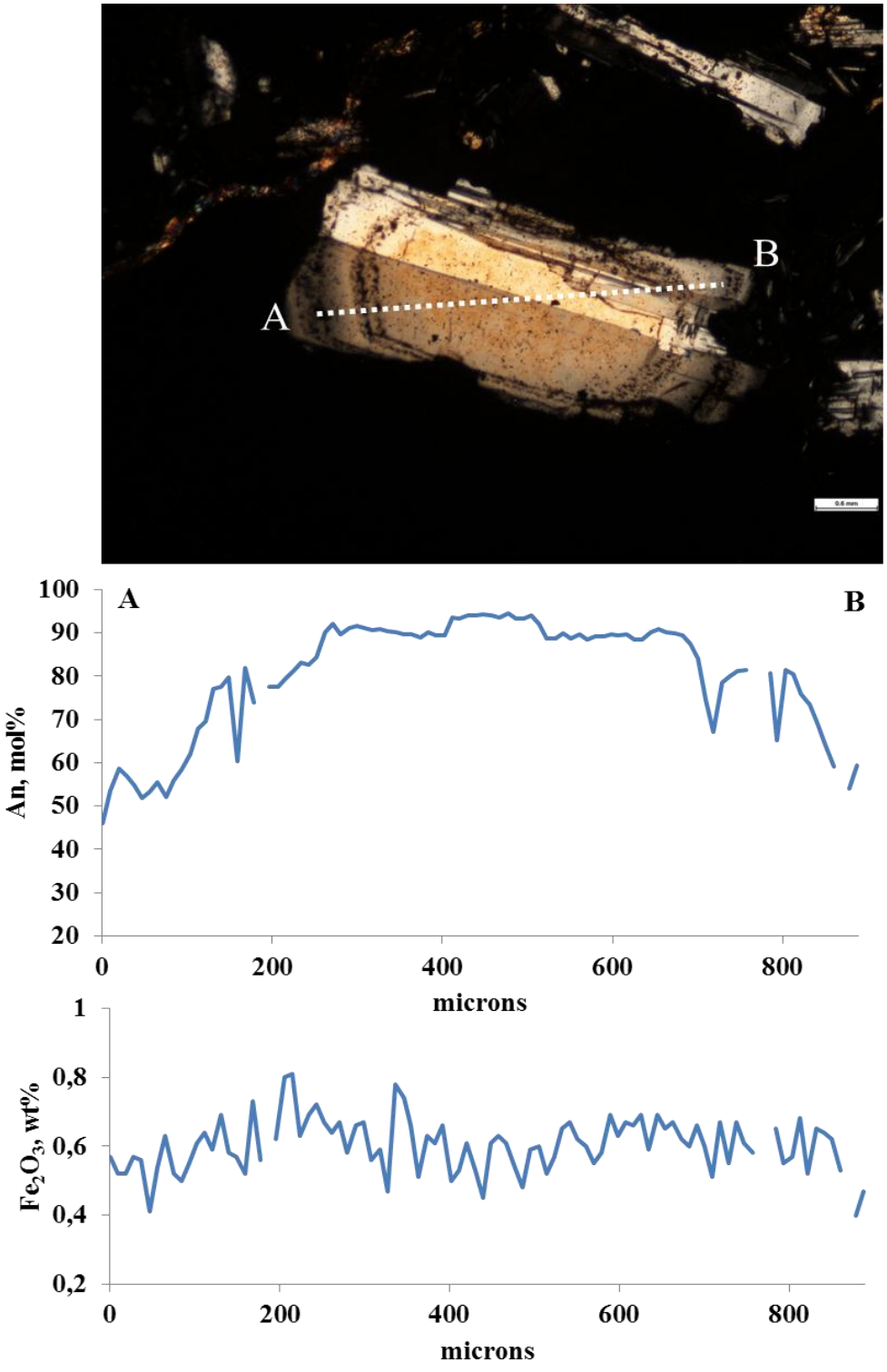

Figure 4 (a). Pyroclastic flow (M 2010 PF) plagioclase phenocryst profiling from A to B points demonstrating extremely enriched in An core (An_{94}). The high-An core is chemical signature of assimilation of sedimentary crustal material (see text). Symmetric chemical zonation in An is spectacular. Fe contents demonstrate oscillatory zonation.

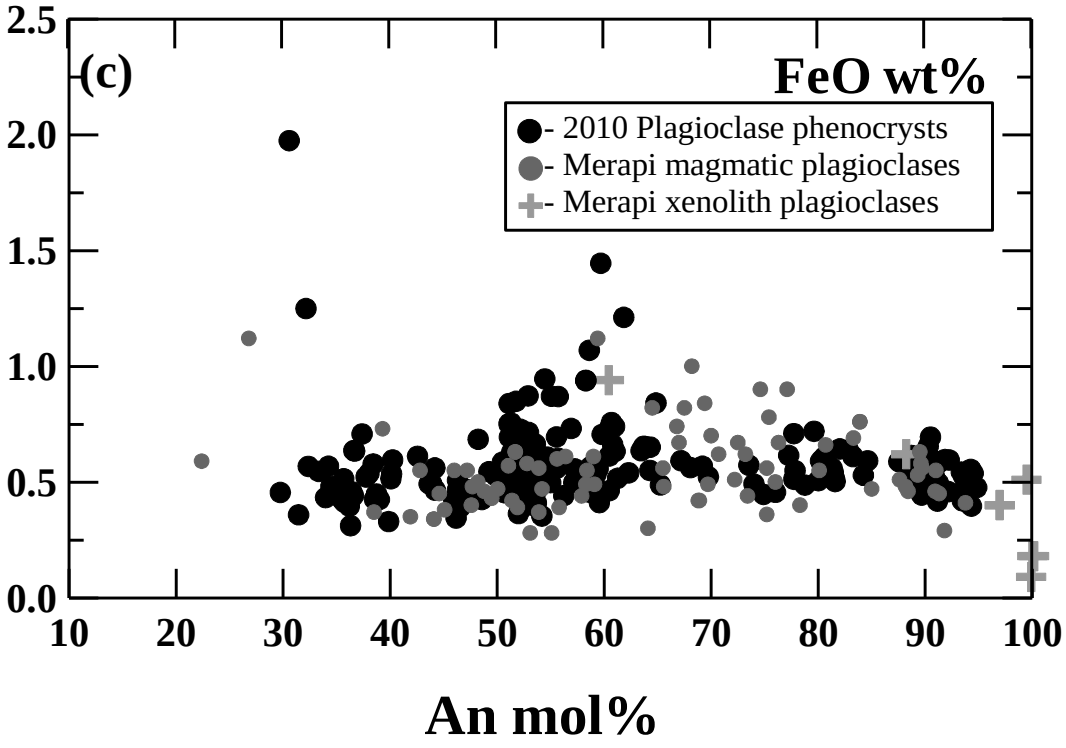

Figure 4(b). The Merapi 2010 plagioclase phenocryst composition compared to typical magmatic plagioclases and calcic plagioclases from the calc-silicate xenoliths. The plagioclase composition for the Merapi volcanic products were obtained from database of MERAPIDATA (Borisova et al., 2011). The database summarizes the published and unpublished data on plagioclases of Berthommier (1990), Camus et al., (2006) for the previous Merapi volcanic products; and Chadwick et al. (2007) for the 1998 Merapi calc-silicate xenoliths. The chemical data on the 2010 Merapi plagioclases are given in Table S2 of ESM.

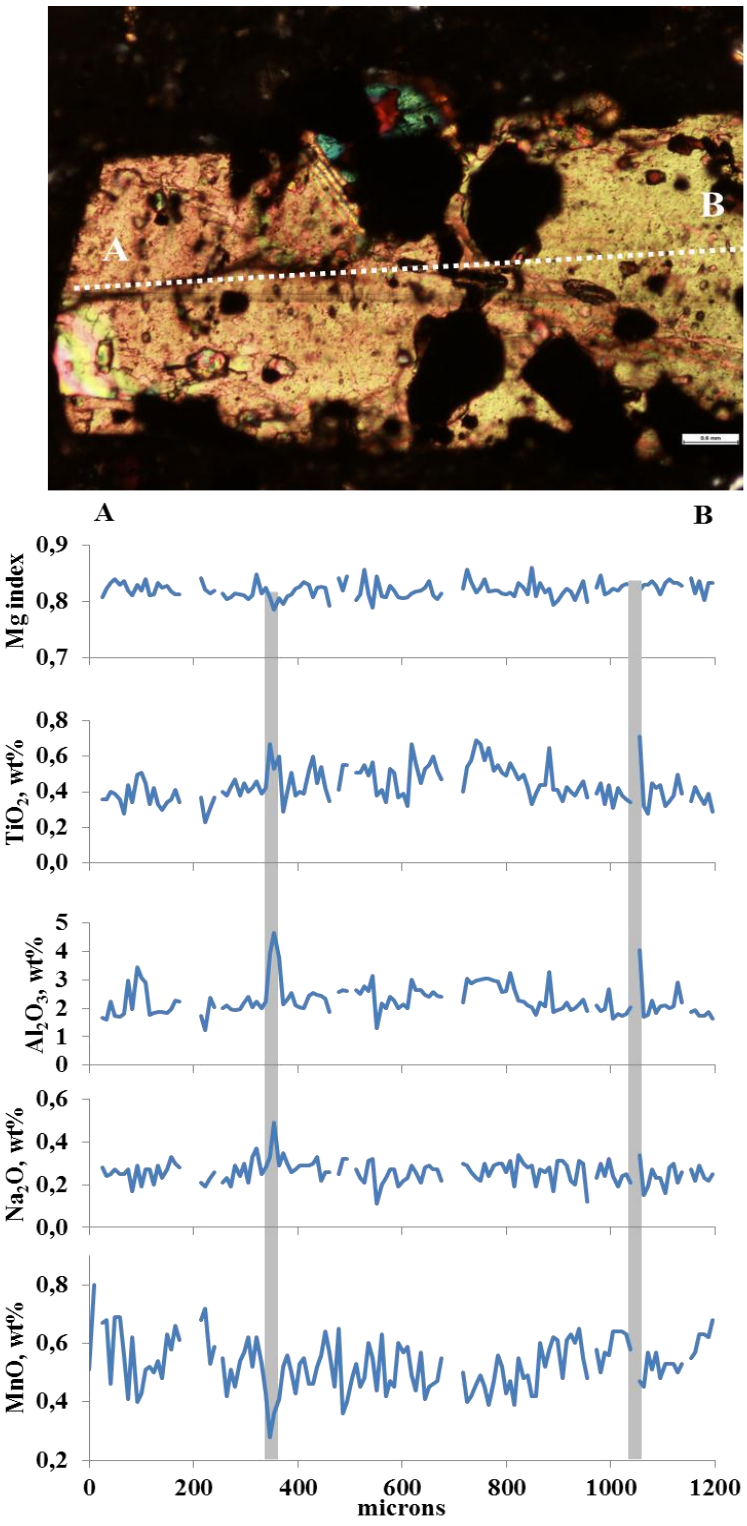

Figure 4 (c). Pyroclastic flow (M 2010 PF) augite phenocryst profiling from A to B points demonstrating oscillatory zonation for trace Al, Ti, Na and Mn. The high-Al -Ti and -Na zones depleted in Mn are marked. The high-Al -Ti and -Na zones indicate crystallization from trachyte melts enriched in alkalis and Al. Numerous inclusions in this crystal have been excluded from the phenocryst zonation. The chemical data on the 2010 Merapi pyroxenes are given in Table S4 of ESM.

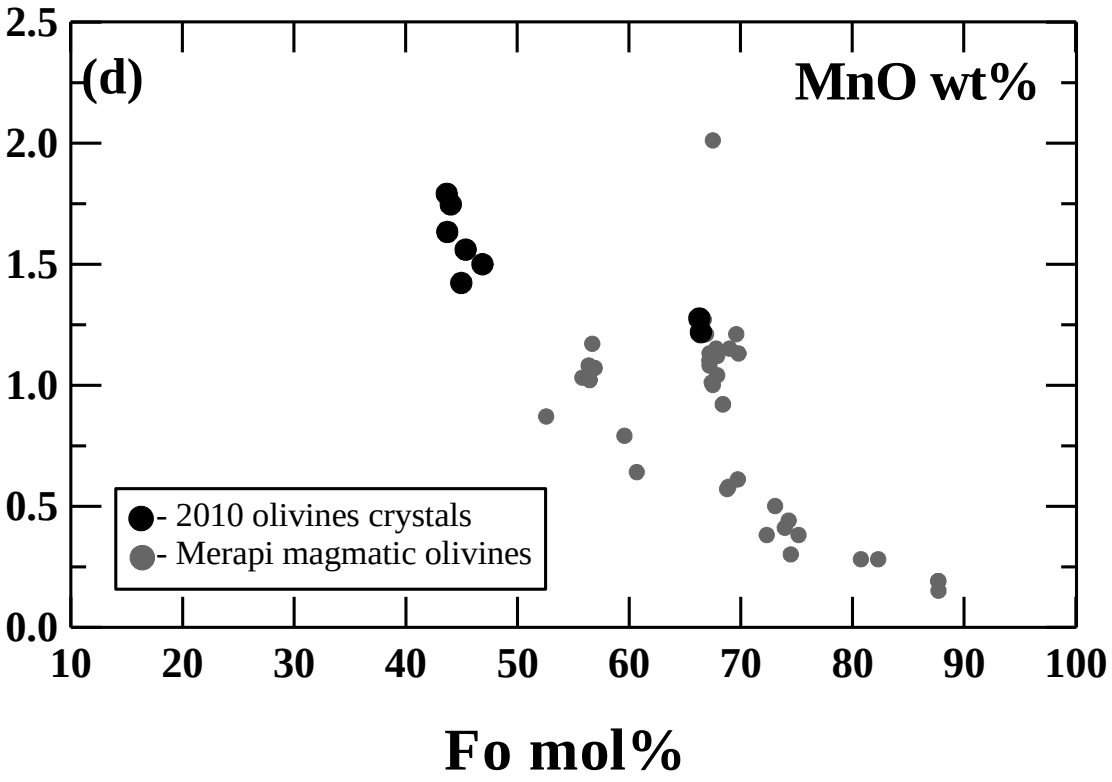

Figure 4(d). The Merapi 2010 olivine composition compared to the typical Merapi olivines. The olivine composition for the Merapi volcanic products were obtained from database of MERAPIDATA (Borisova et al., 2011). The database summarizes the published and unpublished data on olivines of Berthommier (1990), Camus et al., (2006) for the previous Merapi volcanic products. The olivine data on the 2010 Merapi products are given in Table S5 of ESM.

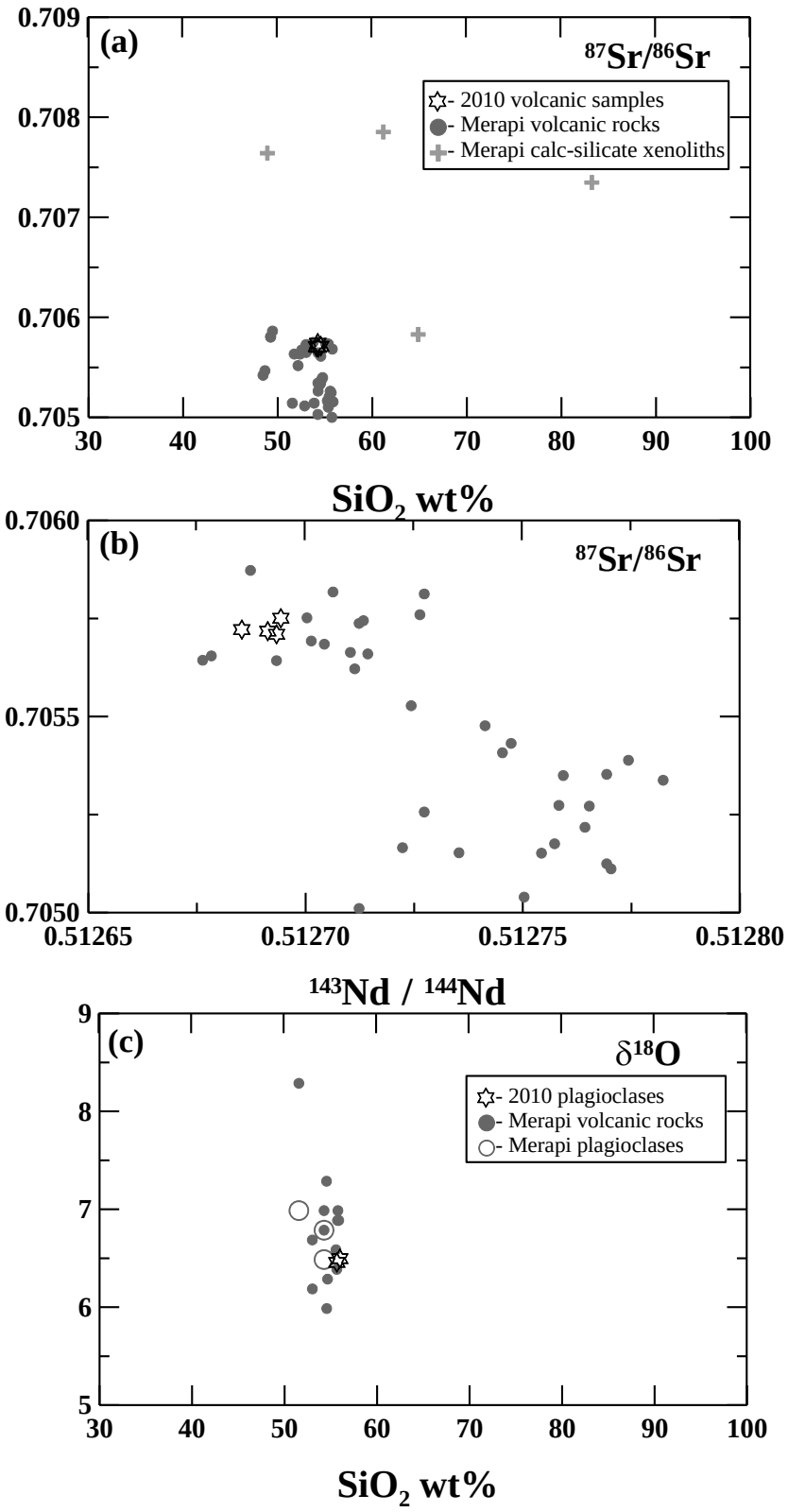

Figure 5. $^{87}Sr/^{86}Sr$ versus (a) SiO_2 in the Merapi bulk rocks; (b) versus $^{143}Nd/^{144}Nd$; (c) $\delta^{18}O$ in plagioclases and bulk rocks versus SiO_2 wt% in the host Merapi rocks. The 2010 Merapi products are characterized by highest $^{87}Sr/^{86}Sr$ ratios approaching those of the calc-silicate xenoliths. The isotopic data used here are obtained from MERAPIDATA (Borisova et al., 2011) which summarize the published isotopic data of Gertisser and Keller (2003a), Debaille et al. (2006) for the previous Merapi volcanic products; and Chadwick et al. (2007) for the 1998 Merapi calc-silicate xenoliths. The isotopic data on the 2010 Merapi are summarized in Table 3.

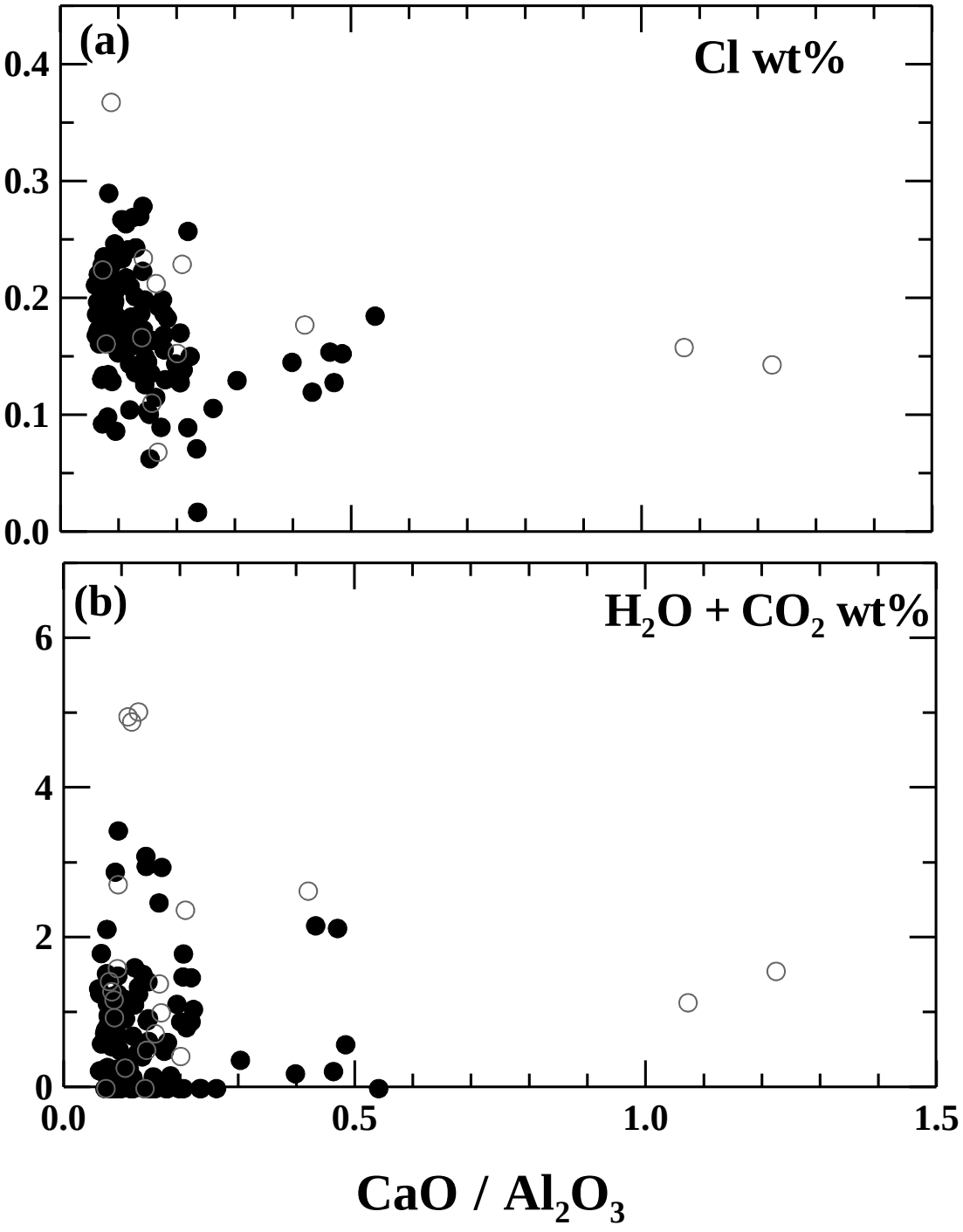

Figure 6. (a) Cl contents and (b) bulk H_2O+CO_2 contents versus CaO/Al_2O_3 in glasses of melt inclusions (open circles) and glassy matrix (closed circles). Bulk H_2O+CO_2 contents in glasses are calculated by-difference method. The melt representing crustal assimilant is characterized by the highest Ca/Al (up to 1.2 wt% of CaO/Al_2O_3), low summary H_2O+CO_2 and low Cl contents. Volatile-richest K-rich melts are characterized by low Ca/Al.

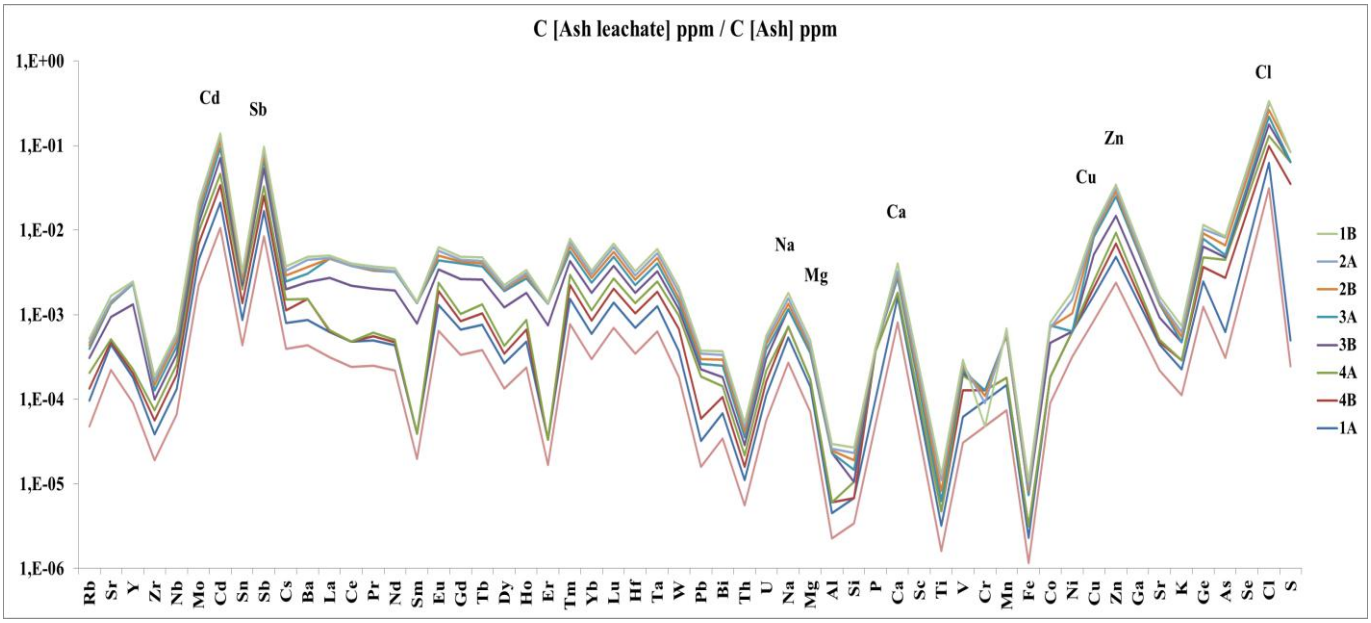

Figure 7. Diagram demonstrating the ash leachate composition normalized to the bulk ash composition for analyzed elements. Positive peaks for Zn, Cu, Cd, Sb and Cl reflect the composition of magmatic fluid liberated during the paroxysmal subplinian eruption in 2010. Chemical data are given in Tables 3 and S6 of ESM.